Front. Eng. Manag. 2025, 12(4): 916–937
https://doi.org/10.1007/s42524-025-4167-2

RESEARCH ARTICLE

Amin BESHARATIYAN, Saeid JOWKAR, Ali ESMAEEL NEZHAD, Ehsan RAHIMI, Fariba ESMAEIL-NEZHAD, Toktam TAVAKKOLI SABOUR, Abbas ZARE, Ayda DEMIR

Tackling optimal power flow in modern power systems using a new optimization strategy

Abstract This paper examines the intricate issue of Optimal Power Flow (OPF) optimization concerning the incorporation of renewable energy sources (RESs) into power networks. We present the Boosting Circulatory System Based Optimization (BCSBO) method, a novel modification of the original Circulatory System Based Optimization (CSBO) algorithm. The BCSBO algorithm has innovative movement techniques that markedly improve its exploration and exploitation skills, making it an effective instrument for addressing intricate optimization challenges. The suggested technique is thoroughly assessed utilizing five different objective functions alongside the IEEE 30-bus and IEEE 118-bus systems as test examples. The performance of the BCSBO algorithm is evaluated against many recognized optimization approaches, including CSBO, Moth-Flame Optimization (MFO), Particle Swarm Optimization (PSO), Thermal Exchange Optimization (TEO), and Elephant Herding Optimization (EHO). For the first case with minimizing the fuel cost associated with the thermal power generators, the total cost reported by the BCBSO is obtained as \$781.8610, which is lower than other algorithms. For the second case, aimed at minimizing the total generating cost while also imposing a fixed carbon tax for thermal units, the derived total cost by the BCBSO is \$810.7654. For the third case, aimed at minimizing the total cost considering prohibited operating zones of thermal units with RESs, the obtained total cost using the BCBSO is \$781.9315. For case 4, with network losses included, the value of total costs obtained using the BCBSO is \$880.4864. The value of total costs considering voltage deviation in case 5 is also obtained as \$961.4354. For the IEEE 118-bus test system, the total cost is obtained \$103,415.9315 using the BCBSO. These values reported by the BCBSO are all lower than those obtained by other methods addressed in this paper. The findings highlight the BCSBO algorithm's potential as a crucial tool for enhancing power systems with renewable energies.

Keywords optimal power flow (OPF), optimization, boosting circulatory system based optimization, solar energy, wind energy

Received Sep. 6, 2024; revised Jan. 3, 2025; accepted Feb. 25, 2025

Amin BESHARATIYAN
Department of Electrical Engineering, Najafabad Branch, Islamic Azad University, Najafabad 8514143131, Iran

Saeid JOWKAR, Abbas ZARE
Department of Electrical, Electronic, and Information Engineering, University of Bologna, Bologna, 40126, Italy

Ali ESMAEEL NEZHAD (✉), Toktam TAVAKKOLI SABOUR, Ayda DEMIR
Department of Electrical and Computer Engineering, Texas Tech University, Lubbock, TX 79409, USA
E-mail: aesmaeel@ttu.edu

Ehsan RAHIMI, Fariba ESMAEILNEZHAD
Young Researchers and Elite Club, Shiraz Branch, Islamic Azad University Shiraz, 7198774731, Iran

1 Introduction

Optimal power flow (OPF) is a useful method for both designing and managing power systems. Since its conception in 1962, the OPF has sparked great interest among academics in electrical network optimization (Esmaeel Nezhad et al., 2022; Ahmadi et al., 2014; Muttaqi et al., 2014). At the core of the OPF challenge is a critical mission: to reveal the essential control settings that beautifully harmonize a symphony of chosen goal functions. These goals, similar to the notes of a grand orchestration, often include the beautiful reduction of fuel costs, pollution expenditures, power losses, and the steady maintenance of an optimum voltage profile. All of this, of course, takes place under the watchful gaze of a complex dance of physical and operational constraints. The decision parameters, akin to the skilled dancers of this performance, encompass a diverse cast of characters: the real power outputs at the generator buses (with the

exception of the master slack bus), the voltage magnitudes gracing every generator node, the artful tap changers within transformers, and the subtle shunt compensators. Together, these elements create a sublime choreography that seeks to attain the apex of operational efficiency and elegance in the realm of power systems (Razavi et al., 2018, Charwand et al., 2016). To tackle OPF problems, numerous mathematical programming methods have been employed, including interior-point methods, Newton-based techniques, linear programming, and nonlinear programming. Nevertheless, traditional techniques employed to tackle the OPF issue lean upon straightforward and differentiable objective functions. Additionally, these methodologies exclusively contemplate thermal power sources as the sole energy providers. In truth, within the sphere of contemporary power systems, the OPF quandary frequently assumes a nonlinear and possibly non-differentiable nature. As a result, it presents a substantial hurdle for optimization methodologies, particularly those of the conventional ilk. In response to these restrictions, heuristic strategies have surfaced as alternative avenues for addressing the OPF puzzle. These methods proffer the advantage of procuring nearly optimal solutions, regardless of the differentiability aspect of the problem.

The conventional OPF problem primarily revolves around power stations that utilize fossil fuels. In the past 20 years, renewable energy sources (RESs) have experienced significant growth, influenced by various factors. These factors encompass increased energy demand, the necessity to reduce greenhouse gas emissions such as NOx and SOx, the progress of deregulation and liberalization in electricity markets, and the appealing cost-efficiency of renewable energy (Javadi et al., 2021; Esmaeel Nezhad et al., 2025). Clearly, wind and solar energy stand out as the most promising alternatives to fossil fuels for power generation. The swift growth in the adoption of RESs can be attributed to the progress in wind power technology (WT) and solar photovoltaic (PV) systems, leading to decreased installation expenses (Esmaeel Nezhad et al., 2024a, Nezhad et al., 2022, Esmaeel Nezhad et al., 2024b)

Over time, heuristic optimization algorithms have emerged as effective solutions to the various optimization problems in various fields of science in the real world like OPF (Naderi et al., 2021) and optimal reactive power dispatch (ORPD) (Saddique et al., 2020; Ghasemi et al., 2022a) optimization problems in the power systems, taking inspiration from natural events, animal behaviors, and evolutionary concepts. A number of these meta-heuristics and optimization algorithms include: liver cancer algorithm (LCA) (Houssein et al., 2023), parrot optimizer (PO) (Lian et al., 2024), slime mold algorithm (SMA) (Li et al., 2020), lungs performance-based optimization (LPO) (Ghasemi et al., 2024b), moth search algorithm (MSA) (Mohamed et al., 2017), hunger games search (HGS) (Yang et al., 2021), geyser inspired Algorithm (GEA) (Ghasemi et al., 2023b), and rime optimization algorithm (RIME) (Su et al., 2023). These algorithms give realistic and effective problem-solving solutions for various OPF problems with different test functions in electrical networks of different sizes. For example, PSOGSA, which combines Particle Swarm Optimization (PSO) and Gravitational Search Algorithm (GSA), has been developed for solving OPF, including FACTS devices and RESs (Hassan et al., 2021), or a new combining Firefly-Bat Algorithm (HFBA-COFS) (Chen et al., 2019a). Optimization studies were conducted to demonstrate the efficacy of the CPSOGSA approach in comparison to other strategies, such as the moth swarm algorithm (MSA), gray wolf optimizer (GWO), and whale optimization algorithm (WOA). Ullah and associates used a hybrid methodology known as PPSOGSA, which blends GSA with phasor PSO (PPSO). In electrical power networks with solar and wind energy sources, this method was used to resolve the OPF problem (Ullah et al., 2019). The use of social spider optimization (SSO) algorithms is a further method for resolving the OPF problem (Nguyen 2019), and the developed GWO (DGWO) (Abdo et al., 2018). In a separate study, Salkuti presented an optimizer to multi-objective OPF (MOOPF) under different operational conditions by the glowworm swarm optimization (GSO) technique and has been tested on the wind energy-integrated IEEE 30-bus and 300-bus electrical networks (Salkuti 2019). There are different algorithms used so far such as Gorilla troops algorithm (GTO) applied to different OPF problems considering uncertainty of RESs in Adrar's isolated power network (Mouassa et al., 2023), INFO algorithm for OPF in hybrid IEEE 30-bus and IEEE 57-bus power networks with RESs (Belagra et al., 2024), a new slim mold optimizer (SMO) used to solve OPF in Algerian electricity network (Mouassa et al., 2022), as well as the self-adaptive bonobo optimizer (SaBO) (Kouadri et al., 2024) and a new enhanced Kepler optimization algorithm (EKOA) (Abid et al., 2024a) for OPF with RESs in the IEEE 30-bus and the Algerian DZA 114-bus power networks, respectively. Also, dwarf mongoose optimizer (DMO) (Mouassa et al., 2024), turbulent flow in water-based optimization (TFWO) (Sarhan et al., 2022; Zahedibialvaei et al., 2023; Alghamdi 2023; Ghasemi et al., 2020), artificial bee colony (ABC) (Mouassa and Bouktir 2015), non-dominated sorting KOA (NSKOA) (Abid et al., 2024b), and whale migration algorithm (WMA) (Ghasemi et al., 2024a) have been deployed for solving various OPF problems in different networks. Additionally, a recently introduced enhanced Honey Bee Mating search algorithm (MHBMO) algorithm, as presented in reference (Niknam et al., 2011), is designed to address the dynamic OPF (DOPF) problem within power systems. This algorithm considers the valve-point effects and has been tested on the 14, 30, and 118-bus electrical networks. The results

demonstrated the effectiveness of MHBMO in solving DOPF.

The algorithm's performance was thoroughly assessed on both the Indian Utility and IEEE 30-bus test systems across a diverse set of optimization functions (Kathiravan and Kumudini Devi 2017) and the DEPSO algorithm (Duman et al., 2020). In (Sarda et al., 2023), a hybrid optimization method named the Cross Entropy-Cuckoo optimization method (CE-CSA) made its debut.

Furthermore, their endeavors extended to deploying the Constrained Multi-Objective Population External Optimization method (CMOPEO) in grappling with the complex OPF issue entwined with wind and solar energy systems. This advanced algorithm underwent rigorous examination within the confines of the IEEE 30-bus test system, subject to an array of diverse test scenarios, as documented in the reference (Chen et al., 2019b). In a parallel line of inquiry, the Chaotic Bonobo Optimizer (CBO) (Hassan et al., 2022) diligently contemplated optimizing three distinct objective functions: minimizing total operating cost, emissions, and power losses. As proposed, the bird swarm algorithm (BSA) by (Ahmad et al., 2021) consistently achieved more stable and accurate outcomes compared to other algorithms.

A novel adaptive Gaussian TLBO (AGTLBO), presented in reference (Alanazi et al., 2022), successfully addressed the OPF problem and significantly enhanced the performance of the conventional TLBO. The results revealed that the AGTLBO exhibited superior efficiency and effectiveness compared to some new approaches mentioned in the existing paper. To grapple with the multifaceted multi-objective challenge, a Multi-objective Electromagnetism-like Algorithm (MOELA) was meticulously crafted, grounded in the principles of Pareto dominance and an external archive strategy. This ingeniously devised approach underwent a rigorous assessment of the well-established IEEE 30-bus electrical network. Another approach worth mentioning is a new TLBO algorithm enhanced with Lévy mutation (LTLBO) (Ghasemi et al., 2015). The efficacy of this approach underwent a comprehensive and systematic investigation involving in-depth scrutiny and rigorous evaluation. This analysis encompassed assessments on the canonical IEEE 30-bus and IEEE 57-bus electrical networks and entailed the consideration of a diverse array of objective functions. It has also been compared to algorithms described in previous studies.

Recently, Ghasemi and his colleagues have designed and successfully proposed a multi-layer intelligent optimization algorithm called circulatory system-based optimization (CSBO) algorithm in 2022 (Ghasemi et al., 2022b). So, in this article, an advanced, improved, and powerful version of this algorithm called the boosting CSBO (BCSBO) algorithm is used to solve and optimize various problems of OPF in a modified standard power system, the IEEE 30-bus network (Biswas et al., 2018). To show the optimization strength of this new effective optimization strategy in solving different OPF problems, we have compared its performance and the obtained simulation results with several powerful modern and new algorithms including particle swarm optimization (PSO), moth-flame optimization (MFO) (Mirjalili 2015), thermal exchange optimization (TEO) (Kaveh and Dadras 2017), and elephant herding optimization (EHO) (Wang et al., 2016) as well as the original version of the CSBO (Ghasemi et al., 2022b).

The suggested new BCSBO-inspired meta-heuristic has shown outstanding performance, especially in search spaces with complex structures and various local solution traps. The BCSBO algorithm has been proven to outperform its competitors through solution studies involving different objective functions and scenarios. The BCSBO has been applied to address OPF, which consists in incorporating RESs into the solution.

The rest of this paper is structured as follows. In Section 2, we provide the formulation of the OPF problem, explicitly focusing on integrating wind and solar energy systems. Section 3 introduces the power models for wind and solar energy. Section 4 is divided into two sub-sections, where we discuss the CSBO and BCSBO algorithms. Additionally, in Section 5, we elucidate the experimental configurations and the benchmark criteria considered during the experimental studies. In the paper's final section, specifically Section 6, we present the study's conclusions and discuss potential future directions for further research.

2 Renewable energy-based OPF modeling

The fundamental objective of OPF is to determine the optimal settings for the control variables, with the overarching goal of minimizing a defined objective function. Concurrently, this optimization endeavor must ensure the fulfillment of both inequality and equality limits. Conventionally the mathematical formulation of this optimization challenge is conventionally articulated as follows (Guvenc et al., 2021):

$$\min f_{\text{obj}}(G,H), \tag{1}$$

subject to:

$$\begin{cases} a(G,H)=0 \\ b(G,H)\leqslant 0 \end{cases}. \tag{2}$$

In the provided expression, f_{obj} (G,H) denotes the OPF problem, while G and H respectively signify the sets of dependent and independent parameters. Furthermore, $a(G,H)$ and $b(G,H)$ represent the equality and inequality limits associated with the problem at hand.

2.1 Dependent variables

G parameters have been given in the below:

$$G=\left[\begin{array}{c}P_{Th_1},V_{L_1},\ldots,V_{L_{NPQ}},Q_{Th_1},\ldots,Q_{Th_{NTHG}},Q_{WS_1},\ldots,Q_{WS_{NW}},\\ Q_{PV_1},\ldots,Q_{PV_{NPV}},S_{L_1},\ldots,S_{L_{NTL}}\end{array}\right]. \tag{3}$$

The location of the operational energy produced by the main power generator is denoted as the slack generator, P_{Th_1}. V_L represents the voltage measurements of the PQ buses, which help determine the reactive power generated by traditional thermal units Q_{Th}, wind power sources Q_{WS}, and the solar system Q_{PV}. Additionally, S_L denotes the overall power transmitted through the lines. In the test power system, *NPQ*, *NTHG*, *NW*, *NPV*, and *NTL* represent the quantities of PQ buses, thermal generating units, wind farms, solar energy systems, and transmission lines respectively.

2.2 *H* parameters

The formulation for the H parameters of OPF has been given as follows.

$$H=[P_{Th_2},\ldots,P_{Th_{NTHG}},P_{WS_1},\ldots,P_{WS_{NW}},P_{PVS_1},\ldots,P_{PVS_{NPV}},V_{G_1},\ldots,V_{G_{NG}}]. \tag{4}$$

In this specific engineering context, P_{Th} symbolizes the active power output from the TH units, excluding the slack generator. Moreover, P_{WS} and P_{PVS} represent the active power contributions generated by WT and PV sources (RESs), respectively. Additionally, V_G corresponds to the voltage magnitudes linked to all generator buses, encompassing the generation units. Lastly, *NG* denotes the numerical count of generator buses, encompassing all the generation units.

2.3 Test system

The specifications and parameters associated with the IEEE 30-bus test system, which includes provisions for wind and solar energy systems, are meticulously detailed in Table 1.

2.3.1 Cost model of the TH generators

The overall expenditure on fuel for all power generation units is expressed using a polynomial quadratic function, as presented in Eq. (5), which depends on the active power output generated. Equation (6) provides the fuel cost model for TH resources taking into account valve-point effects. In this equation, the coefficients m_i, n_i, and o_i describe the costs associated with the ith TH unit, while the coefficients p_i and r_i represent the impact of VPL effects.

Table 1 IEEE 30-bus system parameters

Number	Details	Characteristics
41	Zimmerman et al., (2011)	Branches
30	Zimmerman et al., (2011)	Buses
24	[0.95–1.05] p.u.	PQ bus voltage limits
1	Bus: 1	Swing generators
3	Buses: 1, 2, and 8	TH sources
–	283.4 MW, 126.2 MVAr	Total active and reactive loads
4	Branches: 11, 12, 15, and 36	Transformers
2	Buses: 10 and 24	Shunt capacitor banks
1	Bus: 13	PV sources
11	Generating systems (5 Nos.); voltages of generator buses (6 Nos.)	Control variables
2	Buses: 5 and 11	WT sources

$$CF(P_{Th})=\sum_{i=1}^{NTHG}\left(m_i+n_iP_{Th_i}+o_iP_{Th_i}^2\right), \tag{5}$$

$$CF_1(P_m)=\sum_{i=1}^{NTHG}\left(\begin{array}{c}m_i+n_iP_{m_i}+o_iP_{m_i}^2\\ +\left|p_i\times\sin\left(r_i\times\left(P_{m_i}^{\min}-P_{m_i}\right)\right)\right|\end{array}\right). \tag{6}$$

2.3.2 Emission and carbon tax model

TH plants that utilize different types of fossil fuels emit various harmful pollutants. Recently, one of the main objectives of the OPF is to optimize these emissions while ensuring that the generated power is sufficient to meet the electrical power system's demand. This emission is mathematically represented in Eq. (7) (Guvenc et al., 2021).

In light of the growing apprehension surrounding global climate change, a carbon tax model has been factored into the analysis. The computation of the emission cost entails the summation of the carbon tax value to the total emission value, as succinctly defined in Eq. (8). In this equation, F_E signifies the total emission, C_E denotes the emission cost, and C_{tax} stands for the tax values, respectively (Biswas et al., 2018).

$$F_E=\sum_{i=1}^{NTHG}\left(\begin{array}{c}\left(\sigma_i+\beta_iP_{Th_i}+\tau_iP_{Th_i}^2\right)\times0.01+\\ \omega_ie^{\left(\mu_iP_{Th_i}\right)}\end{array}\right), \tag{7}$$

$$C_E=F_E\times C_{tax}. \tag{8}$$

In the provided context, the symbols σ_i, β_i, τ_i, ω_i, and μ_i correspond to the emission coefficients associated with the ith TH unit.

2.3.3 Forbidden Operational Regions (POZs)

For a TH unit utilizing fossil fuels, the presence of POZs

can be delineated in Eq. (9):

$$\begin{aligned} &P_{Th_{i,\min}} \leqslant P_{Th_i} \leqslant P^L_{Th_{i,1}} \\ &P^U_{Th_{1,y-1}} \leqslant P_{Th_i} \leqslant P^L_{Th_{i,y}} \qquad y = 2,3,4,...,v_i\,. \\ &P^U_{Th_{i,vi}} \leqslant P_{Th_i} \leqslant P^L_{Th_{i,\max}} \end{aligned} \tag{9}$$

In the given equation, "vi " denotes the total count of POZs, "y" represents the specific POZ under consideration, and $P^U_{Th_i,y-1}$ and $P^L_{Th_i,y}$ correspond to the upper and lower limits of the (y−1)th POZ associated with the i-th unit.

Figure 1 graphically illustrates the characteristic curves for fuel cost, delineating the impact of VPEs and the presence of POZs within the thermal generator system.

2.3.4 Direct cost for PVs and WTs

The direct cost model for a wind unit can be concisely formulated as a linear function contingent upon the scheduled power output (Biswas et al., 2018). In this equation, the direct cost function for wind power is denoted as "$DC_{WP,i}$," while the direct cost coefficient is represented by "wsh,i." The scheduled power output from the wind power system is symbolized as $P_{WS,i}$.

$$DC_{WP,i} = CF_{WP,i}P_{WS,i} = wsh,i \times P_{WS,i}. \tag{10}$$

Similarly, the direct cost model for a PV unit has been described by Eq. (11). In the context of the PV system, the direct cost model can be succinctly characterized. The elements within this model encompass the direct cost function for PV power, designated as "$DC_{PV,i}$" the direct cost coefficient denoted by "$pvsh,i$" and the scheduled power output of the PV, represented as "$P_{PVS,i}$" (Guvenc et al., 2021).

$$DC_{PV,i} = CF_{PV,i}(P_{PVS,i}) = pvsh,i \times P_{PVS,i}. \tag{11}$$

2.3.5 Stochastic cost models for PV and WT units

Moving on to uncertainty cost models, the situations of overestimation and underestimation in renewable energy sources have been considered as stochastic cost models for both PV and WT units. Equations (12) and (13) outline the stochastic cost models for WT (Guvenc et al., 2021).

$$\begin{aligned} OC_{WP,i} &= C_{Ow,i}(P_{WS,i} - P_{wav,i}) \\ &= C_{Ow,i}\int_0^{P_{WS,i}} (P_{WS,i} - p_{w,i})\, f_w(p_{w,i})\,\mathrm{d}p_{w,i}, \end{aligned} \tag{12}$$

$$\begin{aligned} UC_{WP,i} &= C_{Uw,i}(P_{wav,i} - P_{WS,i}) \\ &= C_{Uw,i}\int_{P_{WS,i}}^{P_{wr,i}} (p_{w,i} - P_{WS,i})\, f_w(p_{w,i})\,\mathrm{d}p_{w,i}. \end{aligned} \tag{13}$$

In Eqs. (12) and (13), the overestimation and underestimation cost values are represented by $OC_{WP,i}$ and $UC_{WP,i}$, respectively. Additionally, $C_{Ow,i}$ and $C_{Uw,i}$ show the uncertainty cost coefficients while $P_{wr,i}$ and $P_{WS,i}$ show the rated and available active energy of the specific WT. For the models of the PV unit, the mathematical model was obtained using the approach method described in Refs. (Guvenc et al., 2021). The overestimation and underestimation situations are expressed as follows:

$$\begin{aligned} OC_{PV,i} &= C_{Opv,i}(P_{PVS,i} - P_{PVav,i}) = C_{Opv,i} \times f_{PV}(P_{PVav,i} < P_{PVS,i}) \\ &\quad \times [P_{PVS,i} - E(P_{PVav,i} < P_{PVS,i})], \end{aligned} \tag{14}$$

$$\begin{aligned} UC_{PV,i} &= C_{Upv,i}(P_{PVav,i} - P_{PVS,i}) = C_{Upv,i} \times f_{PV}(P_{PVav,i} > P_{PVS,i}) \\ &\quad \times [E(P_{PVav,i} < P_{PVS,i}) - P_{PVS,i}], \end{aligned} \tag{15}$$

where $P_{PVav,i}$ indicates the available power of the ith PV, $C_{Opv,i}$ and $C_{Upv,i}$ represent the uncertainty cost coefficients, and $OC_{PV,i}$ and $UC_{PV,i}$ describe the over- and underestimation cost values.

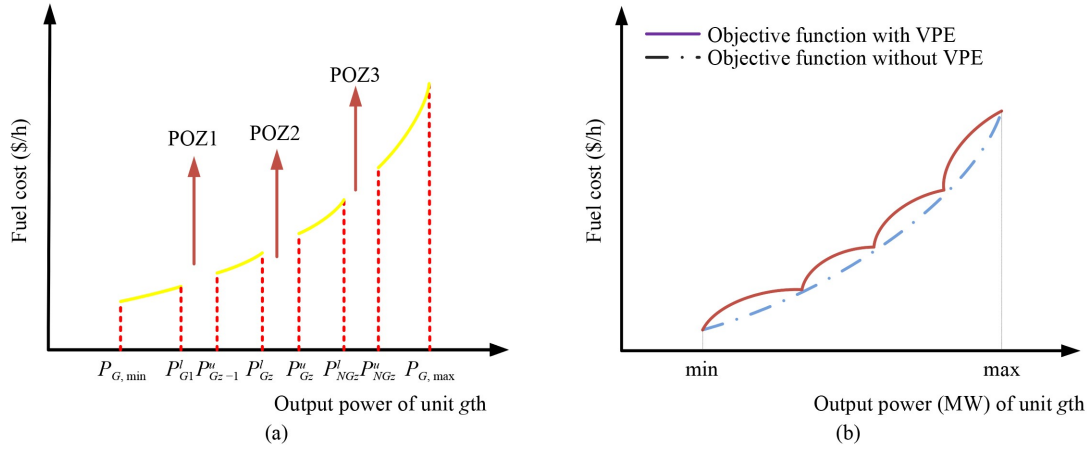

Fig. 1 Fuel cost curves: (a) without and with VPE, (b) with POZs.

2.4 Objective functions

2.4.1 VPEs considering fuel cost objective function

Eqation (16) represents the modeled cost of OPF. This function encompasses the cost values associated with the VPEs of the TH units, as well as the cost values of the PV and WT units.

$$F_{obj1} = CF_1(P_{th}) + \sum_{i=1}^{NW}(DC_{WP,i} + OC_{WP,i} + UC_{WP,i}) + \sum_{i=1}^{NPV}(DC_{PV,i} + OC_{PV,i} + UC_{PV,i}). \tag{16}$$

2.4.2 Objective functions considering tax and emission

The defined objective function for the formulated OPF is precisely outlined in Eq. (17)

$$F_{obj2} = F_{obj1} + C_E. \tag{17}$$

2.4.3 Objective function considering POZs

Here, the conventional OPF objective function associated with TH units featuring POZs has been introduced as the designated OPF function, as expressed in Eq. (18).

$$F_{obj3} = CF(P_{th}) + \sum_{i=1}^{NW}(DC_{WP,i} + OC_{WP,i} + UC_{WP,i}) + \sum_{i=1}^{NPV}(DC_{PV,i} + OC_{PV,i} + UC_{PV,i}). \tag{18}$$

2.4.4 Network losses

The minimizing of the network losses of the electrical network is considered as follows:

$$F_{obj4} = P_{loss} = \sum_{s=1}^{NTL} G_{s(ij)}\left(V_i^2 + V_j^2 - 2V_iV_j\cos(\delta_{ij})\right). \tag{19}$$

In the given equation, "$G_{s(ij)}$" corresponds to the conductance of the s-th transmission line linking buses i and j, while δ_{ij} quantifies the voltage angle differential between buses i and j.

2.4.5 Voltage deviation (*VD*)

The proposed OPF problem utilizes a calculation, as demonstrated in Eq. (20), to determine the voltage deviation value of contemporary electrical grids.

$$F_{obj5} = VD = \sum_{i=1}^{NPQ}\left|V_{L_i} - 1\right|. \tag{20}$$

2.5 OPF constraints

2.5.1 Equality constraints

The equality constraints inherent to the formulated OPF can be aptly expressed as follows:

$$P_{Gi} - P_{Di} - V_i\sum_{j=1}^{N_{\text{bus}}} V_j(G_{ij}\cos(\delta_i - \delta_j) + B_{ij}\sin(\delta_i - \delta_j)) = 0, \tag{21}$$

$$Q_{Gi} + Q_{SHi} - Q_{Di} - V_i\sum_{j=1}^{Nbus} V_j(G_{ij}\sin(\delta_i - \delta_j) - B_{ij}\cos(\delta_i - \delta_j)) = 0. \tag{22}$$

In the context of these equations, various variables and parameters hold significance:

- P_{Gi}, and P_{Di} show the active power outputs of the ith generating unit, encompassing thermal, wind, and PV units, as well as the load buses.
- Q_{Gi}, Q_{SHi}, and Q_{Di} characterize the reactive power contributions from the ith generating unit, including thermal, wind, and PV units, shunt VAR compensators, and load buses within the electrical grid.
- N_{bus} stands for the total count of buses within the power system.
- V_i and V_j represent the voltage magnitudes at the ith and jth buses.
- $\delta_i - \delta_j$ signifies the angular disparity between the voltage phasor values at the ith and jth buses.
- G_{ij} and B_{ij} describe the conductance and susceptance attributes governing the transmission line connecting the ith and jth buses.

2.5.2 Inequality limits

1) Generator limits

The boundaries for the permissible ranges of active and reactive power, and voltage magnitudes for all the generators are explicitly specified and denoted in Eq. (23).

$$\begin{cases} P_{Th_i,\min} \leqslant P_{Th_i,\max} & i = 1:NTHG \\ P_{WS_i,\min} \leqslant P_{WS_i} \leqslant P_{WS_i,\max} & i = 1:NW \\ P_{PV_i,\min} \leqslant P_{PV_i} \leqslant P_{PV_i,\max} & i = 1:NPV \\ Q_{Th_i,\min} \leqslant Q_{Th_i} \leqslant Q_{Th_i,\max} & i = 1:NTHG \\ Q_{iWS_i,\min} \leqslant Q_{WS_i} \leqslant Q_{WS_i,\max} & i = 1:NW \\ Q_{PV_i,\min} \leqslant Q_{PV_i} \leqslant Q_{PV_i,\max} & i = 1:NPV \\ V_{G_i,\min} \leqslant V_{G_i} \leqslant V_{G_i,\max} & i = 1:NG \end{cases} \tag{23}$$

2) Security limits

The voltage magnitude at each of the PQ-type buses must conform to specified boundaries, and the apparent power flow on each transmission line is subject to constraints related to its maximum capacity. In these equations, "$V_{L_i,\min}$" and "$V_{L_i,\max}$" respectively denote the down and upper limits of the voltage for the ith PQ bus, while "S_{L_i}" and "$S_{L_i,\max}$" represent the apparent power and the maximum apparent power capacity for the ith transmission line.

$$\begin{cases} V_{L_i,\min} \leqslant V_{L_i} \leqslant V_{L_i,\max} & i = 1:NPQ \\ S_{L_i} \leqslant S_{L_i,\max} & i = 1:NTL \end{cases}. \tag{24}$$

The fitness function for SCOPF, encompassing thermal, PV, and WT power units, can be succinctly described as presented in Eq. (25). Where λ_{VPQ}, λ_{Pslack}, λ_{QTH}, λ_{QWS}, λ_{QPV}, and λ_{SL} are the penalty coefficients.

$$\begin{aligned} J = {} & f_{ab_r}(G,H) + \lambda_{rp_0}\sum_{i=1}^{NPO}(VL_i - VL_i^{im})^2 + \lambda_{p_{i-1}}(P_{m_1} - P_{m_1}^{im})^2 \\ & + \lambda_{om}\sum_{i=1}^{NTHG}(Q_{n_i} - Q_{n_i}^{im})^2 + \lambda_{ows}\sum_{i=1}^{NW}(Q_{ns_i} - Q_{ns_i}^{im})^2 \\ & + \lambda_{0PV}\sum_{i=1}^{NPV}(Q_{PV_i} - Q_{PV_i}^{in})^2 + \lambda_{SL}\sum_{i=1}^{NTL}(S_{L_i} - S_{L_i}^{in})^2. \end{aligned} \tag{25}$$

3 Wind-PV uncertainty and power models

The distribution for wind speed has been characterized by the Weibull probability density function (PDF), as elucidated in Eq. (26). Within this equation, "vw" signifies the wind speed, while "ξ" and "ψ" represent the shape and scale factors, respectively (Biswas et al., 2017; Guvenc et al., 2021).

$$f_v(v_w) = \left(\frac{\xi}{\psi}\right)\left(\frac{v_w}{\psi}\right)^{\xi-1}\left(e^{-\left(\frac{v_w}{\psi}\right)^{\xi}}\right). \tag{26}$$

In Fig. 2, you can see the outcomes of the Weibull fitting for wind frequency distributions. These results were generated using an 8000-iteration Monte Carlo simulation (Guvenc et al., 2021). The identified method for determining the output power of the WT is as follows:

$$p_w(v_w) = \begin{cases} 0 & v_w \leqslant v_{w,w} \text{ and } v_w > v_{w,w} \\ \left(\dfrac{v_w - v_{w,w}}{v_{w,w} - v_{w,w}}\right) * p_w & v_{w,w} \leqslant v_w \leqslant v_{w,w} \\ p_{w,w} & v_{w,w} \leqslant v_w \leqslant v_{w,w} \\ 0 & v \geqslant v_{w,w} \end{cases}, \tag{27}$$

where p_{wr}, $v_{w,in}$, $v_{w,out}$, and $v_{w,r}$ show, respectively, the rated power, cut-in, cut-out and rated wind speeds. The energy production of a WT system is partitioned into discrete intervals contingent upon wind speeds, as delineated in Eq. (27). The associated probability values for these intervals are meticulously elaborated between Eqs. (28) and (30).

$$f_-(p_-)\{p_- = 0\} = 1 - \exp\left(-\left(\frac{v_{-\text{in}}}{\psi}\right)^2\right) + \exp\left(-\left(\frac{v_{-\text{in}}}{\psi}\right)^2\right), \tag{28}$$

$$f_w(p_w)\{p_w = p_w\} = \exp\left(-\left(\frac{v_{w,x}}{\psi}\right)^2\right) - \exp\left(-\left(\frac{v_{w,\text{out}}}{\psi}\right)^2\right), \tag{29}$$

$$f_w(p_w) = \left[\frac{\xi(v_{w,\text{r}} - v_{w,\text{in}})}{\psi^{\xi} p_{wr}}\right] \times \left(v_{w,\text{in}} + \left(\frac{p_w}{p_{wr}}\right)(v_{w,\text{r}} - v_{w,\text{in}})\right)^{\xi-1} \times \exp\left(-\left(\frac{v_{w,\text{in}} + \left(\frac{p_w}{p_{wr}}\right)(v_{w,\text{r}} - v_{w,\text{in}})}{\psi}\right)^{\xi}\right). \tag{30}$$

The power production of a wind farm is partitioned into discrete intervals contingent upon wind speeds, as delineated in Eq. (27). The associated probability values for these intervals are meticulously elaborated between Eqs. (28) and (30), respectively (Guvenc et al., 2021).

To express the power output of the PV energy systems in relation to solar irradiation, the Lognormal PDF was utilized. The mathematical representation of the probabilistic model and output power of the solar system can be observed in Eqs. (31) and (32) (Guvenc et al., 2021).

$$f_{G_{PV}}(G_{PV}) = \frac{1}{G_{PV}\Omega\sqrt{2\pi}}\exp\left(\frac{-(\ln G_{PV} - \xi)^2}{2\Omega^2}\right) \text{ for } G_{PV} > 0. \tag{31}$$

In Fig. 3, you can observe the frequency distribution and lognormal probability of solar irradiation, which were obtained through an 8000-iteration Monte Carlo simulation.

$$P_{PV_0} = \begin{cases} P_{PV_{\text{rate}}} \times \left(\dfrac{G_{PV}}{G_{PV} \times R_C}\right) \text{ for } 0 < G_{PV} < R_C \\ P_{PV_{\text{rate}}} \times \left(\dfrac{G_{PV}}{G_{PV_{\text{std}}}}\right) \text{ for } G_{PV} \geqslant R_C \end{cases}. \tag{32}$$

The Lognormal PDF is characterized by the mean (ζ) and standard deviation (Ω) values, as illustrated in Table 2. In this context, G_{PV}, $G_{PV_{\text{std}}}$ and $P_{PV_{\text{rate}}}$ refer to the probability value, standard solar irradiance, and rated power of the solar system, respectively. At bus 13, these

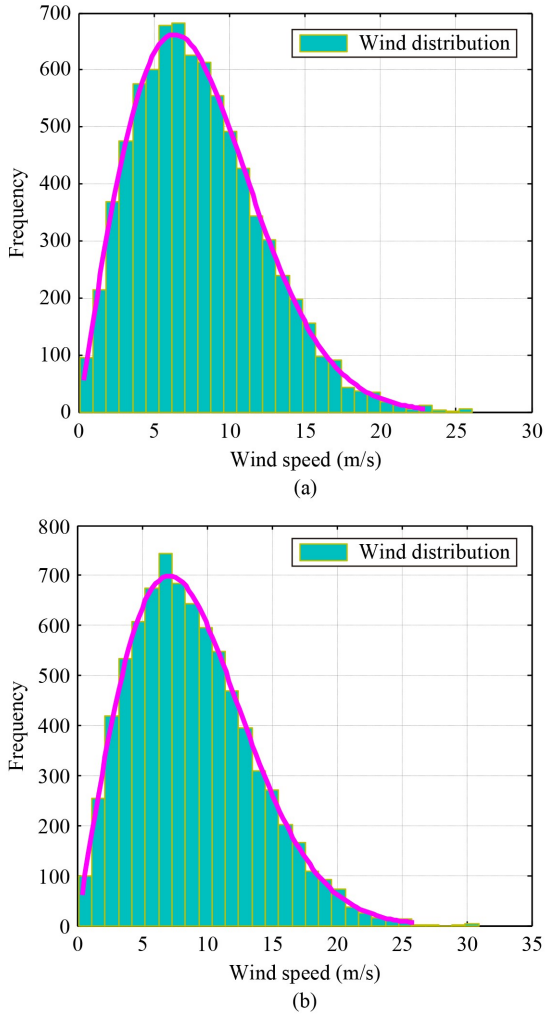

Fig. 2 The data of the Weibull fitting for wind frequency distributions for wind generator at (a) bus 5 and (b) bus 11.

values are defined as 800 W/m^2 and 50 MW. Additionally, the R_C value is set at 120 W/m^2. Figure 4 displays a histogram representing the stochastic output power of PV. The line on the graph represents the intended power that PV is designed to transmit to the system. It can be very vital to note that the planned PV power is a variable quantity.

4 Improved meta-heuristic

4.1 The original meta-heuristic

4.1.1 CSBO algorithm

Initially, the CSBO algorithm, similar to other meta-heuristic algorithms, commences by creating an initial population known as blood masses BM_i. This population is tailored to address a specific problem and consists of dimensions D and $Npop$. The values of the problem parameters are randomly generated within the minimum

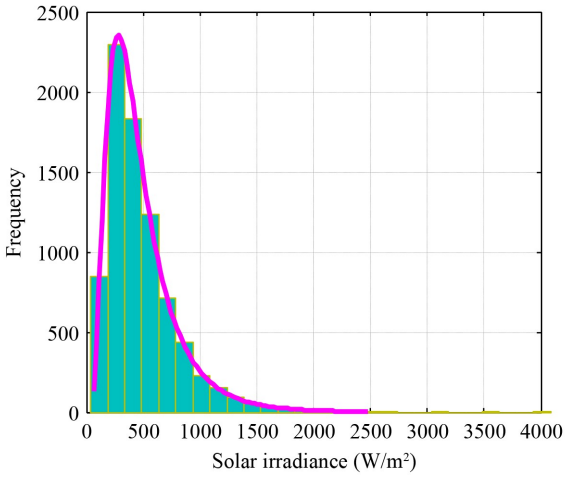

Fig. 3 The PDF for solar irradiance, modeled as a lognormal distribution, as it pertains to the solar PV generator situated at bus 13.

$BM_{\min}$ and maximum $BM_{\max}$ values, similar to Eq. (33). This initial population, akin to blood particles or masses within the body, fulfills a crucial role as previously mentioned.

$$BM_i = BM_{\min} + \text{rand}(1, D) \times (BM_{\max} - BM_{\min}) \quad i = 1 : Npop. \tag{33}$$

4.1.2 Movement of blood mass in the veins

In the circulatory system, each blood mass flowing through the veins, referred to as BM_i, is influenced by an external force or pressure. As it moves, the mass always seeks to find a path with more favorable conditions, aiming to minimize its objective function (the amount of force or pressure it experiences). The phenomenon of clogged arteries in the heart can be understood as the entrapment of blood masses in local optimal solutions. However, in order to avoid such situations in reality, it is crucial for the body to continuously optimize the circulatory process. This particular stage of the circulatory cycle is accurately represented by modeling the positions of particles and their corresponding objective function values.

$$BM_i^{\text{new}} = BM_i + K_{i1} \times p_i \times (BM_i - BM_1) + K_{23} \times p_i \times (BM_3 - BM_2) \ . \tag{34}$$

$$K_{ij} = \frac{F(BM_j) - F(BM_i)}{\left|F(BM_j) - F(BM_i)\right| + \varepsilon} \ . \tag{35}$$

4.1.3 Population or blood mass flow in pulmonary circulation

As previously stated, the pulmonary system is responsible

Table 2 displays the parameters of the PDFs for the PV and WT units

WT in bus 5			WT in bus 11			PV in bus 13	
Weibull PDF parameters	Total rated power (P_{wr})	Number of turbines	Weibull parameters	Total rated power (P_{wr})	Number of turbines	Lognormal parameters	Rated power (P_{PVrate})
$\xi = 2, \psi = 9$	75 MW	25	$\xi = 2, \psi = 10$	60 MW	20	$\zeta = 6, \Omega = 0.6$	50 MW

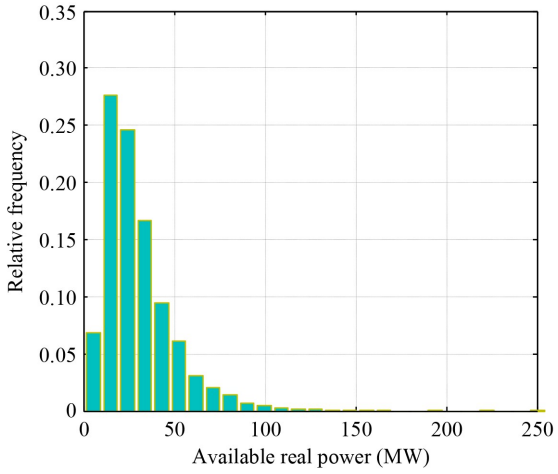

Fig. 4 Solar power distribution at node 13.

for handling deoxygenated blood, comparable to a lesser population in the context of optimization. Specifically, within the CSBO framework, during each iteration, the population undergoes sorting, and a certain number *NR* of the most vulnerable individuals enter the pulmonary circulation. These individuals are then directed toward the lungs to acquire oxygen.

$$BM_i^{new} = BM_i + \left(\frac{randn}{it}\right) \times randc(1, D), \quad i = 1 : NR. \quad (36)$$

In the equation above, the term "*randn*" represents a random number sampled from a normal distribution, "*it*" signifies the current iteration within the algorithm, "*randc*" designates a random vector originating from the Cauchy probability distribution, and "*D*" stands for the dimensionality of the optimization problem. Additionally, the pulmonary circulation modifies the "*p*" value for this population in the following manner:

$$p_i = \text{rand}(1, D), \quad i = 1 : NR. \quad (37)$$

4.1.4 Population or blood mass flow in systematic circulation

As previously noted, a specific count of the weakest sorted population members, denoted as *NR*, are introduced into the pulmonary circulation. Concurrently, the remaining portion of the population, represented by *NL* (*NL* = *Npop* - *NR*), and possessing superior fitness values, are channeled into the systemic circulation. These individuals receive a fresh allocation to circulate throughout the system, as illustrated in the model below:

$$\begin{aligned} &\text{for } j = 1 : D \\ &if\ rand > 0.9 \\ &BM_{i,j}^{\text{new}} = BM_{1,j} + p_i * (BM_{3,j} - BM_{2,j}) \\ &\text{else} \\ &BM_{i,j}^{\text{new}} = BM_{i,j} \\ &\text{end} \\ &\text{end} \\ &i = 1 : NL \end{aligned} \quad . \quad (38)$$

The systemic circulation likewise adjusts the "*p*" value for this subgroup of the population in the subsequent manner:

$$p_i = \frac{F(BM_i) - F_{\text{Worst}}}{F_{\text{Best}} - F_{\text{Worst}}}, \quad i = 1 : NL. \quad (39)$$

In this context, "F_{Worst}" and "F_{Best}" respectively represent the most unfavorable and optimal values of the cost function achieved up to the current iteration. The optimization procedure will continue for the predetermined number of iterations. Much like other meta-heuristic algorithms, each member within the population will adopt the novel position solely if it results in an improved objective function value. The pseudo-code for the CSBO has been succinctly encapsulated in Algorithm 1, as depicted in Table 3, also, to further understand the framework of the proposed extended optimization strategy and optimization code, the flowchart of this proposed strategy is presented in Fig. 5.

4.2 Boosting circulatory system-based optimization

The original CSBO algorithm faced challenges in quickly converging and avoiding local optima, especially for complex problems like economic load dispatch. To address these issues and enhance the algorithm's performance, we introduced improved strategies outlined in Eqs. (40) and (41). Through experiments and simulations, we consistently observed that our proposed BCSBO algorithm outperformed the original CSBO algorithm. Specifically, we incorporated additional vectors in the blood movement and population flow phase in systematic circulation, i.e., $K_{54} \times p_i \times (BM_5 - BM_4)$ and $p_i \times (Bm_{5,j} - Bm_{4,j})$, which significantly improved the algorithm's effectiveness. The results demonstrate the positive impact of these

Table 3 The CSBO algorithm pseudo-code

Algorithm 1: CSBO

1: /* Initialization */

2: for $i = 1 : Npop$

3: $BM_i = BM(BMmin_{\max};)_{\min}$

4: $F(BM_i) = Cost(BM_i)$;

5: $NFE = NFE + 1$.

6: end

7: /* The main cycle */

8: /* Movement of blood mass in the veins */

9: for $i = 1 : Npop$

10: $BM_i^{new} = BM_i + K_{i1} * p_i * (BM_i - BM_1) + K_{23} * p_i * (BM_3 - BM_2)$;

11: if $F\left(BM_i^{new}\right) \leqslant F(BM_i)$

12: $BM_i = BM_i^{new}$;

13: $F(BM_i) = F\left(BM_i^{new}\right)$;

14: end

15: $NFE = NFE + 1$.

16: end

17: Sort the population from the **best to worst**.

18: /* Population flow in Pulmonary Circulation*/

19: for $i = 1 : NR$

20: $BM_i^{\text{new}} = BM_i + \left(\frac{randn}{it}\right) * randc(1, D)$;

21: if $F\left(BM_i^{\text{new}}\right) \leqslant F(BM_i)$

22: $BM_i = BM_i^{new}$;

23: $F(BM_i) = F\left(BM_i^{new}\right)$;

24: end

25: $NFE = NFE + 1$.

26: end

27: /* Population flow in Systematic Circulation */

28: for $i = 1 : NL$

29: for $j = 1 : D$

30: if $rand > 0.9$

31: $Bm_{i,j}^{\text{new}} = Bm_{1,j} + p_i * \left(Bm_{3,j} - Bm_{2,j}\right)$

32: else

33: $Bm_{i,j}^{\text{new}} = Bm_{i,j}$

34: end

35: end

36: if $F\left(BM_i^{\text{new}}\right) \leqslant F(BM_i)$

37: $BM_i = BM_i^{\text{new}}$;

38: $F(BM_i) = F\left(BM_i^{\text{new}}\right)$;

39: end

40: $NFE = NFE + 1$.

41: end

42: **repeat** the main cycle until terminal condition.

auxiliary vectors on enhancing the original algorithm.

Improvements made on CSBO to achieve a power optimizer (BCSBO):

A new boosting movement of blood mass in the veins strategy:

$$BM_i^{\text{new}} = BM_i + K_{i1} \times p_i \times (BM_i - BM_1) + K_{23} \times p_i \times (BM_3 - BM_2) + K_{54} \times p_i \times (BM_5 - BM_4). \quad (40)$$

The proposed boosting population flow in systematic circulation strategy:

$$Bm_{i,j}^{\text{new}} = Bm_{1,j} + p_i \times (Bm_{3,j} - Bm_{2,j}) + p_i \times (Bm_{5,j} - Bm_{4,j}). \quad (41)$$

5 Solving OPF by the proposed meta-heuristic method

5.1 OPF in the IEEE 30-bus test system

We have done a study on the fundamental CSBO, EHO, TEO, MFO, PSO, and BCSBO techniques using the IEEE 30-bus test system, as illustrated in Fig. 6. Our objective was to address the OPF problem in the presence of wind and solar energy systems. Additionally, we have obtained the control parameters for the optimization algorithms from relevant references, which are presented in Table 4. The system parameters for the IEEE 30-bus test system were obtained from the following references: (Guvenc et al., 2021; Biswas et al., 2017; Mohamed et al., 2017), and are provided in Table 5.

Table 6 displays the cost coefficients for overestimation and underestimation of wind and solar power systems. To calculate the load flow equations for the OPF, which encompasses thermal, wind, and solar generating systems, MATPOWER (Zimmerman et al., 2011) was employed. To statistically assess the simulation results obtained, all optimization algorithms were executed 30 times for each test case of the proposed OPF problem. The simulation studies were conducted based on the test cases outlined below.

5.2 Case 1: Optimizing the fuel cost with VPEs with RESs

In this particular scenario, the aim is to minimize the fuel cost associated with the thermal power generators. Table 7 provides a detailed comparison of control parameters and their respective optimum values attained by six algorithms: EHO, TEO, MFO, PSO, CSBO, and the suggested BCSBO technique. The main objective is to reduce gasoline expenses while complying with all issue limits. The table presents the optimal, suboptimal (Max), mean (Mean), and standard deviation (Std.) values derived from 30 different executions of each method, offering a comprehensive statistical evaluation. The

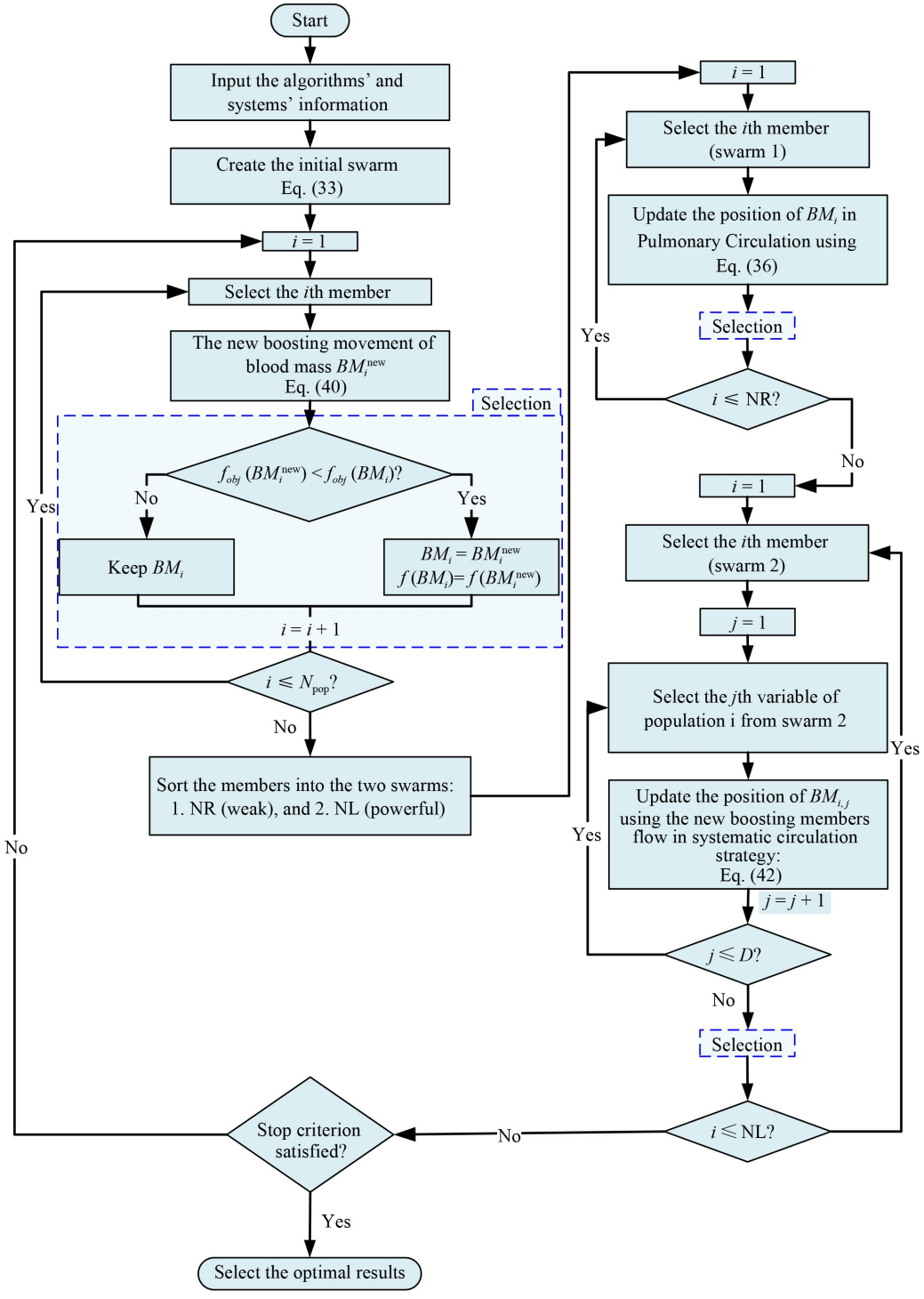

Fig. 5 The performance framework of the proposed optimization strategy.

findings underscore the BCSBO method's superior performance in attaining the lowest objective function value relative to all other algorithms. This supremacy reflects the algorithm's ability to efficiently explore and utilize the search space. Moreover, the BCSBO algorithm exhibits reliable performance, as shown by its minimal standard deviation and its capacity to avoid constraint breaches. The primary benefit of the proposed BCSBO technique is its capacity to maintain a balance between exploration and exploitation, shown by its smooth convergence curve toward the ideal solution, seen in Fig. 7. In contrast to other methods that may demonstrate oscillations or slower convergence rates, the BCSBO approach attains rapid convergence to a high-quality

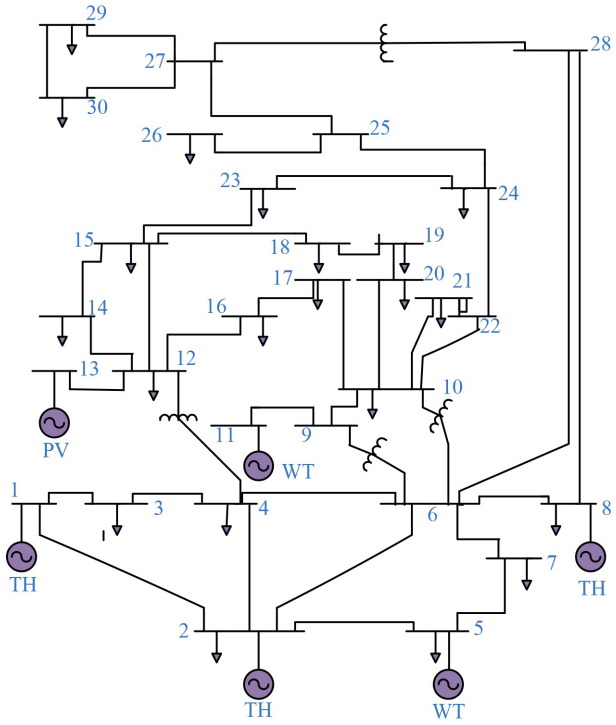

Fig. 6 IEEE 30-bus system.

solution with minimum processing resources.

5.3 Case 2: Optimizing the total cost with emission and carbon tax

The main objective of this particular case is to optimize the overall generating cost while also imposing a fixed carbon tax (C_{tax}) on the TH units due to their CO2 emissions, as mentioned in Eq. (8). The designated forced carbon tax is set at 20 ($/ton) (Biswas et al., 2017). Table 8 provides a detailed comparison of the control parameters and optimum values identified by many sophisticated optimization techniques, including EHO, TEO, MFO, PSO, CSBO, and the suggested BCSBO approach. This table elucidates the efficacy of different algorithms in tackling the OPF issue, emphasizing cost reduction while complying with system restrictions.

Table 4 The decision variables of the meta-heuristics

Meta-heuristics	*Decision variables*
EHO	$\alpha = 0.5$
	$\beta = 0.1$
	Kept elephants number = 2
	Elephants number = 60
	Clans number = 5
MFO	Moth-flame number = 60
	$b = 1$
	$a = [-2 : -1]$
TEO	$c_1, c_2 = 1$
	$TMs = 3$
	Objects number = 60
PSO	Population size = 60
	$C_1 = [0.5 \rightarrow 2.5]$
	$C_2 = [2.5 \rightarrow 0.5]$
	$w = [0.899 \rightarrow 0.399]$
CSBO and BCSBO	$NR = 15$
	Population size = 60

Table 8 highlights a significant finding: all algorithms, including the suggested BCSBO approach, attained the minimum overall cost of 810.7654 ($/h). This exceptional result underscores the competitive efficacy of the BCSBO algorithm. What distinguishes the BCSBO technique is its exceptional ability to optimize efficiently while ensuring solution feasibility under established restrictions. A further notable aspect of the BCSBO algorithm's performance is shown in Fig. 8, which demonstrates the method's convergence behavior. The quick and seamless convergence curve demonstrates the algorithm's efficacy in attaining the ideal answer. This swift convergence illustrates the algorithm's computing efficiency and highlights its resilience in balancing exploration and exploitation throughout the optimization phase. The BCSBO method's constant attainment of high-quality solutions, shown via its performance in several iterations, establishes it as a dependable and potent instrument for

Table 5 The objective function's characteristics for the electrical network

Bus no	TH	*m*	*n*	*R*	*p*	*o*	*τ*	*ω*	*σ*	*μ*	*B*	*POZs*
1	1	0	2	0.037	18	0.00375	6.49	0.0002	4.091	6.667	− 5.554	Ghasemi et al., (2024a)
2	2	0	1.75	0.038	16	0.0175	5.638	0.0005	2.543	3.333	− 6.047	Ghasemi et al., (2024a)
8	3	0	3.25	0.045	12	0.00834	3.38	0.002	5.326	2	− 3.55	Ghasemi et al., (2024a)

Table 6 The cost characteristics of the PV and WT resources

WT1				WT2				PV			
Bus 5	*wsh,1*	$C_{Uw,1}$	$C_{Ow,1}$	Bus 11	*wsh,2*	$C_{Uw,2}$	$C_{Ow,2}$	Bus 13	$C_{Upv,1}$	$C_{Opv,1}$	*pvsh,1*
	1.60	1.5	3		1.75	1.5	3		1.5	3	1.60

Table 7 The optimal values of variables obtained for case 1

Variables	Min	Max	EHO	TEO	MFO	PSO	CSBO	BCSBO
P_{Th1} (MW)	50	140	134.90791	134.90791	134.90791	134.90791	134.90791	134.90791
P_{Th2}	20	80	29.3917	29.002	29.17	27.0233	28.0842	28.8755
P_{WS1}	0	75	44.262	44.0141	44.106	42.9149	43.5077	43.9456
P_{Th3}	10	35	10	10	10	10	10	10
P_{WS2}	10	30	37.335	37.1535	37.2285	36.2472	36.7402	37.0887
P_{PV}	0	50	33.3687	34.0919	33.755	38.1007	35.9419	34.3485
V_1 (p.u.)	0.95	1.1	1.0721	1.0718	1.0718	1.072	1.0715	1.0724
V_2	0.95	1.1	0.9528	1.0568	1.0569	1.0569	1.0566	1.0575
V_5	0.95	1.1	1.0364	1.0349	1.035	1.0348	1.0346	1.0354
V_8	0.95	1.1	1.0593	1.0996	1.0563	1.0396	1.0894	1.0398
V_{11}	0.95	1.1	1.1	1.0989	1.0981	1.0982	1.0983	1.0982
V_{13}	0.95	1.1	1.0996	1.0489	1.0488	1.0556	1.0493	1.0544
Q_{Th1} (Mvar)	−20	150	14.4352	−2.32079	−2.3092	−1.99863	−2.38843	−1.88328
Q_{Th2}	−20	60	−20	11.8173	11.8334	13.1684	11.7337	13.28
Q_{WS1}	−30	35	28.658	22.4183	22.4169	23.2231	22.424	23.173
Q_{Th3}	−15	40	40	40	40	34.9293	40	35.1349
Q_{WS2}	−10	50	29.3857	30	30	30	30	30
Q_{PV}	−20	25	25	15.0894	15.0614	17.7288	15.2573	17.2755
Fuel cost ($/h)	–	–	443.5435	442.2406	442.8016	435.6903	439.1887	441.8186
Wind gen cost ($/h)	–	–	249.3674	247.8779	248.4560	240.9927	244.7060	247.4170
Solar gen cost ($/h)	–	–	89.6791	92.3374	91.2925	105.4811	98.2385	92.6255
Total Cost ($/h)	–	–	782.5899	782.4559	782.5501	782.1642	782.1333	781.8610
Emission (t/h)	–	–	1.76187	1.76196	1.76192	1.76245	1.76218	1.76199
Power losses (MW)	–	–	5.8653	5.7695	5.7674	5.7940	5.7819	5.7663
V.D. (p.u.)	–	–	0.53945	0.45407	0.45395	0.46496	0.45476	0.46281
Mean	–	–	783.6629	783.6812	783.9528	782.6746	782.3527	781.9722
Max	–	–	784.7318	784.6940	785.1263	783.8962	782.5801	782.1356
Std.	–	–	2.37	1.72	3.69	1.48	0.67	0.12
Time (s)	–	–	28	31	36	22	27	25

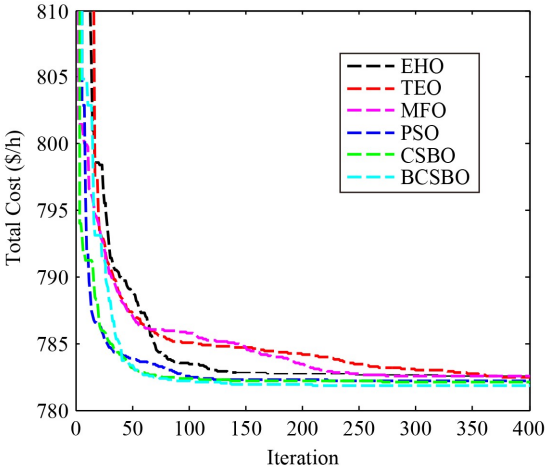

Fig. 7 Convergence trajectories of different methods for case 1.

tackling intricate OPF challenges. Its efficiency, along with its adaptation to varied system circumstances, guarantees its relevance in numerous energy optimization contexts. The results shown in Table 8, together with the convergence analysis in Fig. 8, unequivocally demonstrate that the BCSBO approach is the most efficient optimizer for the OPF issue in this research. Its capacity to provide optimum solutions with efficiency and reliability highlights its potential for further applications in energy system optimization.

5.4 Case 3: Optimizing the total cost considering POZs of TH units with RESs

Table 9 presents a comprehensive study of the control parameters and results associated with total cost minimization, including the impact of restricted operating

Table 8 The optimal values of variables obtained for case 2

Variables	EHO	TEO	MFO	PSO	CSBO	BCSBO
P_{Th1} (MW)	123.98861	123.93020	122.88694	123.91626	123.41260	123.87498
P_{Th2}	34.3513	34.2205	30.9701	34.1872	32.7822	34.0113
P_{WS1}	46.6935	46.6678	45.0801	46.609	45.9216	46.5247
P_{Th3}	10	10	10.0014	10	10	10
P_{WS2}	39.2809	39.2409	37.8274	39.2294	38.6448	39.1524
P_{PV}	34.3649	34.711	41.9208	34.8393	38.0055	35.1145
V_1 (p.u.)	1.071	1.0722	1.0689	1.0713	1.0718	1.0709
V_2	1.0575	0.9543	1.0559	0.9516	0.9551	1.0574
V_5	1.0364	1.0391	1.0362	1.0998	1.0385	1.0363
V_8	1.0405	1.0458	1.0675	1.0499	1.0659	1.0405
V_{11}	1.1	1.1	1.0988	1.0996	1.1	1.099
V_{13}	1.0549	1.0639	1.0512	1.0588	1.0648	1.0552
Q_{Th1} (Mvar)	−2.54459	15.5544	−4.62491	12.3636	15.3354	−2.54937
Q_{Th2}	12.428	−20	10.9151	−20	−20	12.3581
Q_{WS1}	22.9478	29.7986	23.5775	35	29.7116	22.9333
Q_{Th3}	35.419	40	40	40	40	35.4064
Q_{WS2}	30	30	30	30	30	30
Q_{PV}	17.4166	20.7054	15.8704	18.6578	21.0016	17.5106
Fuel cost ($/h)	435.1010	434.5117	420.9486	434.3638	428.3464	433.6585
Wind gen cost ($/h)	264.8382	264.6025	253.9498	264.3491	259.8059	263.7708
Solar gen cost ($/h)	93.4343	94.2245	119.5461	94.3990	105.4400	95.1486
Emission (t/h)	0.91531	0.91225	0.85969	0.91152	0.88567	0.90938
Carbon tax ($/h)	18.3062	18.245	17.1938	18.2304	17.7134	18.1876
Total cost ($/h)	811.6797	811.5837	811.6383	811.3423	811.3058	810.7654
Power losses (MW)	5.2793	5.3703	5.2868	5.3811	5.3667	5.2778
V.D. (p.u.)	0.46728	0.50152	0.46321	0.48982	0.50365	0.46781
Mean	812.8549	813.0701	813.3811	812.5410	811.8100	810.8809
Max	814.2536	815.2999	815.3074	813.1461	812.2539	810.9647
Std.	2.08	2.67	1.76	1.01	0.61	0.23
Time (s)	27	35	36	32	30	31

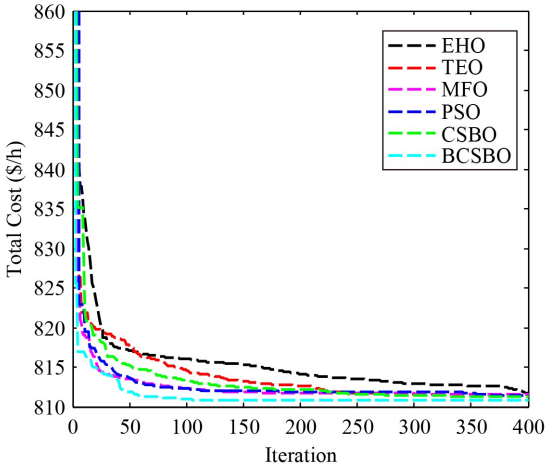

Fig. 8 Convergence trajectories of different methods for case 2.

zones (POZs) for thermal units and the incorporation of wind-PV energy systems. The findings were obtained utilizing the suggested BCSBO algorithm in conjunction with several alternative methodologies, enabling a comprehensive comparison across 50 separate trials. Table 9 unequivocally illustrates the BCSBO algorithm's enhanced efficacy in minimizing power losses and optimizing expenses. The BCSBO approach specifically achieved a minimal power loss of 781.9315 $/h, surpassing all rival algorithms. This underscores the algorithm's capacity to adeptly manage the difficulties posed by the POZ limitations and the incorporation of renewable energy sources, demonstrating its efficacy in practical energy optimization contexts. Besides its quantitative benefits, the convergence characteristics of the BCSBO algorithm are shown in Fig. 9. The convergence curve of

Table 9 The optimal values of variables obtained for case 3

Variables	EHO	TEO	MFO	PSO	CSBO	BCSBO
P_{Th1} (MW)	134.90791	134.90791	134.90791	134.90791	134.90791	134.90791
P_{Th2}	29.3513	27.133	27.615	27.1535	28.3229	28.8983
P_{WS1}	44.2029	42.9767	43.2546	42.9872	43.6766	43.9503
P_{Th3}	10	10	10	10	10	10
P_{WS2}	37.303	36.2988	36.5314	36.3148	36.847	37.1041
P_{PV}	33.4004	37.8757	36.8747	37.8335	35.5163	34.3104
V_1 (p.u.)	1.0718	1.072	1.0721	1.0713	1.0736	1.0717
V_2	1.0569	1.057	1.0571	1.0563	0.966	1.0568
V_5	1.035	1.0348	1.035	1.0342	1.0379	1.0349
V_8	1.0604	1.0397	1.0397	1.0496	1.0453	1.0515
V_{11}	1.0998	1.0994	1.0989	1.0996	1.0998	1.0997
V_{13}	1.0487	1.0555	1.0553	1.0499	1.0635	1.049
Q_{Th1} (Mvar)	−2.3023	−1.96609	−1.95381	−2.43986	16.6858	−2.3531
Q_{Th2}	11.876	13.15	13.1756	11.6276	−20	11.7756
Q_{WS1}	22.4068	23.2334	23.1822	22.4341	30.1191	22.4612
Q_{Th3}	40	34.9487	35.0213	40	40	40
Q_{WS2}	30	30	30	30	30	30
Q_{PV}	15.0208	17.6783	17.5933	15.4497	20.601	15.1222
Fuel cost ($/h)	443.4080	436.0505	437.6375	436.1180	439.9801	441.8945
Wind gen cost ($/h)	249.0506	241.3788	243.1223	241.4691	245.6552	247.4861
Solar gen cost ($/h)	90.2066	105.0969	101.7669	104.4918	96.4325	92.5508
Total cost ($/h)	782.6652	782.5262	782.5267	782.0789	782.0679	**781.9315**
Emission (t/h)	134.90791	1.76242	1.76230	1.76242	1.76213	1.76199
Power losses (MW)	5.7655	5.7921	5.7837	5.7969	5.8707	5.7710
V.D. (p.u.)	0.45377	0.46469	0.46440	0.45567	0.49550	0.45426
Mean	783.7058	783.7845	783.8491	782.9743	782.7115	**782.0852**
Max	784.6992	785.1006	785.3457	783.7948	783.3205	**782.1766**
Std.	2.64	2.75	3.41	1.97	1.32	**0.75**
Time (s)	30	31	33	25	26	27

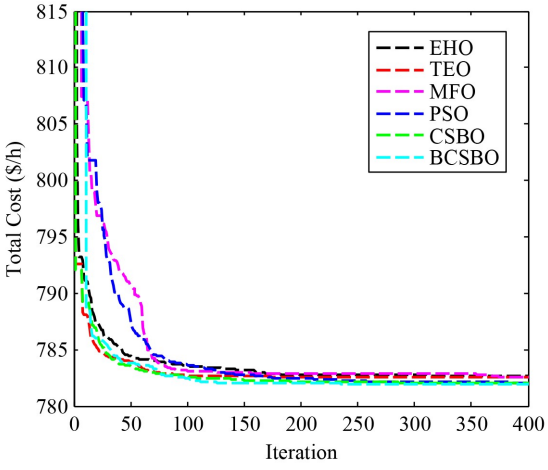

Fig. 9 Convergence trajectories of different methods for case 3.

the BCSBO approach demonstrates a notable superiority over other algorithms, characterized by its swift advancement toward the ideal solution. This behavior highlights the algorithm's efficacy in balancing exploration and exploitation, facilitating a seamless and expedited convergence process. The incorporation of POZ limitations and renewable energy systems adds considerable complexity to the optimization issue, necessitating resilient and adaptable optimization methodologies. The BCSBO algorithm's consistent performance over several separate executions reinforces its dependability and robustness in tackling these difficulties. The findings in Table 9, corroborated by the convergence traits shown in Fig. 9, confirm that the BCSBO algorithm is an exceptionally efficient and dependable approach for optimizing energy systems with complex constraints. Its capacity to reduce costs and power losses while ensuring fast conver-

gence makes it an essential instrument for addressing intricate power system optimization challenges.

5.5 Case 4: Considering network losses

The results for the decision parameters and total cost obtained from the innovative BCSBO algorithm for case 4 can be found in Table 10. This table also displays the optimal outcomes after conducting 30 independent implementations, along with the time taken to achieve the best result using the proposed BCSBO algorithm and other methods for case 4. Table 10 clearly demonstrates that the proposed BCSBO method attains the best value of (2.0741 MW), which is lower than the values obtained by other methods. Moreover, the standard deviation achieved by the proposed BCSBO algorithm (0.20) is significantly smaller compared to both the original CSBO algorithm (0.46) and the other methods. Additionally, Fig. 10 illustrates the convergence characteristic of the proposed BCSBO and other optimizers for this particular case. The BCSBO algorithm exhibits smoother convergence curves when compared to alternative algorithms.

5.6 Case 5: Optimizing V.D

Table 11 presents a comprehensive study of the decision parameters and voltage deviation (V.D.) derived from the IEEE 30-bus system including RESs using the proposed BCSBO algorithm. The table presents the findings from 30 separate simulation runs, contrasting the BCSBO approach with other optimization strategies. Table 11 illustrates the advantages of the BCSBO algorithm in reducing V.D. and attaining optimum system performance. The BCSBO method has superior results for

Table 10 The optimal values of variables for case 4

Variables	EHO	TEO	MFO	PSO	CSBO	BCSBO
P_{Th1} (MW)	50.13336	50.06827	50.35701	50.65479	50.00	50.00
P_{Th2}	25.8784	28.8565	22.3209	28.681	30.0654	25.0512
P_{WS1}	74.8096	74.9049	74.8482	74.8667	75	75
P_{Th3}	34.0854	34.8571	33.1257	34.5382	35	35
P_{WS2}	57.9377	59.7058	59.0621	56.9344	60	59.9999
P_{PV}	43.1859	44.06	46.3185	39.887	40.4752	40.423
V_1 (p.u.)	1.032	0.9607	1.0356	1.0514	0.9792	1.0581
V_2	1.0514	1.0518	1.0527	1.0484	1.0546	1.0527
V_5	1.046	1.0741	1.0542	1.0447	1.0454	1.0435
V_8	1.0556	1.0552	1.0646	1.0569	1.0777	1.0934
V_{11}	1.0849	1.0949	1.0808	1.0963	1.0999	1.0964
V_{13}	1.0773	1.0611	1.0651	1.0401	1.0631	1.0567
Q_{Th1} (MVAR)	−20	−20	−20	−10.1224	−20	−5.23183
Q_{Th2}	14.8847	7.04812	12.5962	8.8501	19.0244	6.41139
Q_{WS1}	24.1521	35	31.434	26.928	20.7427	20.4894
Q_{Th3}	40	40	40	40	40	40
Q_{WS2}	25.1008	28.6338	24.0383	30	30	30
Q_{PV}	25	18.9476	21.521	13.677	19.5567	17.6644
Fuel cost ($/h)	301.4043	314.1502	286.8136	450.6397	318.5736	302.0429
Wind gen cost ($/h)	454.7466	462.9132	459.8343	450.6397	464.6295	464.6293
Solar gen cost ($/h)	124.5381	127.0405	136.4541	112.6560	114.8907	113.8142
Total cost ($/h)	880.6891	904.1039	883.1019	877.3488	898.0938	880.4864
Emission (t/h)	0.09882	0.09800	0.10002	0.09833	0.09768	0.09895
Power losses (MW)	2.1720	2.1781	2.2026	2.1620	2.1037	2.0741
V.D. (p.u.)	0.54229	0.54001	0.51511	0.43519	0.54676	0.50843
Mean	3.1524	3.0849	3.2790	2.7389	2.3542	2.2284
Max	3.8935	3.9775	4.0005	3.3476	2.7478	2.3799
Std.	1.04	1.25	1.87	1.11	0.46	0.20
Time (s)	31	33	30	27	28	28

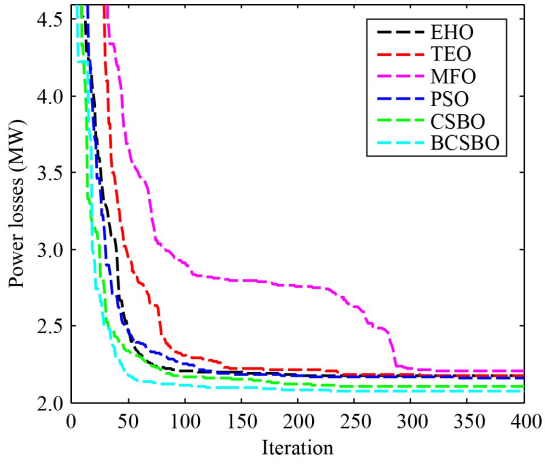

Fig. 10 Convergence trajectories of different methods for case 4.

essential statistical metrics, including standard deviation (Std.), indicating its consistency and resilience throughout several iterations. These results highlight the method's efficacy in tackling the issues presented by the OPF problem in systems with integrated RESs. Additionally, Fig. 11 depicts the convergence characteristics of the proposed BCSBO algorithm in relation to other approaches. The convergence behavior of BCSBO demonstrates a swift and seamless progression toward the optimum solution, highlighting its efficacy in traversing the intricate optimization terrain of the OPF problem. The stability and rapid convergence further confirm the robustness of the BCSBO algorithm in harmonizing exploration and exploitation throughout the optimization process. The use of renewable energy sources in the IEEE 30-bus system brings complications, including intermittent power production and integration limits,

Table 11 The optimal values of variables for case 5

Variables	EHO	TEO	MFO	PSO	CSBO	BCSBO
P_{Th1} (MW)	82.39454	93.56642	87.52856	79.34532	76.18067	75.22631
P_{Th2}	76.5891	77.7182	76.5167	73.107	79.4708	80
P_{WS1}	67.0998	57.5369	65.8142	73.6627	74.9436	75
P_{Th3}	33.0625	31.6636	33.5041	32.5783	34.8959	35
P_{WS2}	31.9569	26.1234	31.8695	27.7641	22.3315	22.5681
P_{PV}	0.68	2.9772	1.7025	1.5296	0.0645	0
V_1 (p.u.)	0.9641	0.977	0.9904	1.0078	1.048	1.0376
V_2	1.0876	1.0863	1.0827	1.0936	1.0868	1.1
V_5	0.9933	0.9906	0.992	0.9948	0.9961	0.9961
V_8	1.0643	1.0817	1.0989	1.0811	1.0488	1.1
V_{11}	1.0907	1.0944	1.0942	1.0918	1.0962	1.0927
V_{13}	1.0974	1.0785	1.0626	1.0695	1.0751	1.0594
Q_{Th1} (Mvar)	−20	−20	−20	−20	−20	−20
Q_{Th2}	60	60	60	60	60	60
Q_{WS1}	−18.3232	−16.9725	−17.4831	−19.7634	−19.5703	−19.6326
Q_{Th3}	40	40	40	40	40	40
Q_{WS2}	29.7538	30	30	29.9876	30	30
Q_{PV}	25	25	25	25	25	25
Fuel cost ($/h)	583.9912	613.8551	599.9681	559.0491	585.2755	585.0750
Wind gen cost ($/h)	321.9916	265.4444	316.2351	338.2266	330.0362	330.8370
Solar gen cost ($/h)	45.3432	45.4629	45.6676	45.0322	46.3056	45.5234
Total cost ($/h)	951.3259	924.7624	961.8708	942.3079	961.6174	961.4354
Emission (t/h)	0.15552	0.21647	0.17811	0.14356	0.13744	0.13533
Power losses (MW)	4.6533	5.2440	4.6417	4.4228	4.4736	4.4504
V.D. (p.u.)	0.37828	0.38020	0.37896	0.37792	0.37585	**0.37576**
Mean	0.38425	0.39183	0.38876	0.38214	0.38005	**0.37681**
Max	0.39812	0.47269	0.45633	0.39310	0.38986	**0.37949**
Std.	0.10	0.13	0.097	0.084	0.035	**0.012**
Time (s)	31	33	30	27	28	30

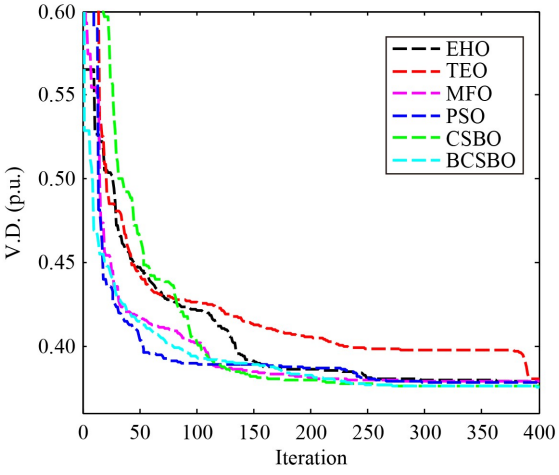

Fig. 11 Convergence trajectories of different methods for case 5.

necessitating that optimization methods be both adaptable and efficient. The findings indicate that the BCSBO approach not only achieves reduced voltage variations but also sustains consistent and steady performance, even under adverse settings. The results from Table 11, corroborated by the convergence trends in Fig. 11, decisively affirm the BCSBO algorithm as a highly efficient and resilient optimizer for addressing the OPF issue in power systems with renewable energy sources. Its capacity to get optimal results while facilitating fast convergence makes it an essential instrument for improving the efficiency and dependability of contemporary power networks.

5.7 Case 6: OPF in IEEE 118-bus test system

In the following simulation, we have implemented the optimization methods in the previous section, CSBO, EHO, TEO, MFO, PSO, and BCSBO techniques, on the IEEE 118-bus test system to test and demonstrate the performance and efficiency of the proposed improved metaheuristic for the various OPF problems (Duman et al., 2020; Ghasemi et al., 2023a). The best choice for the various control parameters of the algorithms used is the same as in the previous section, with the difference that the selected population for the algorithms is 75 and the number of iterations of the algorithms is 2000. The system parameters for the IEEE 118-bus test system were obtained from the following references (Duman et al., 2020; Ghasemi et al., 2023a).

Nine transformers, two reactors, 12 shunt capacitors, 50-four generators, and 186 branches make up the test network under analysis (Duman et al., 2020; Ghasemi et al., 2023a). The reactive power injections of 12 capacitors, nine transformer tap settings, the active power output of 54 generators, and bus voltage levels are among the 129 parameters that are optimized. The reactive power provided by the capacitors spans from 0 to 30 Mvar. All buses have their voltage levels kept between 0.94 and 1.06 per unit, transformer taps are calibrated between 0.90 and 1.10 per unit (Duman et al., 2020). This system integrates RESs across many busses. Solar power units are situated at buses 6, 15, and 34, and wind turbines are strategically located at busses 18, 32, 36, 55, 104, and 110 (Alghamdi and Zohdy, 2024). The optimal outcomes attained by several algorithms in this investigation are shown in Table 12. An examination of this table clearly indicates that the suggested technique exhibits enhanced optimization performance as the dimensions of the test network expand, unlike the majority of other methods. Consequently, it can be said that the strategy described in this paper is a successful and significant approach for future research initiatives. In addition, convergence trajectories of different methods for the IEEE 118-bus test system have been shown in Fig. 12. From this figure, it can be seen that, with increasing complexity and dimension of the OPF problem under consideration, the proposed BCSBO method still has a good convergence characteristic and is very competitive, especially compared to the initial optimization CSBO method.

5.8 Discussion

The performance of the BCSBO algorithm is evaluated against various meta-heuristic approaches under the same optimization circumstances, with results shown in Tables 7 to 12. Although the numerical findings indicate that BCSBO excels in attaining lower objective function values and quicker convergence in the majority of instances, a more profound comprehension of its behavior elucidates the underlying causes for these outcomes.

5.8.1 Efficiency of blood mass movement in Veins

The algorithm's capacity to model the dynamic flow of blood masses under pressure guarantees a thorough investigation of the search space. This approach avoids premature convergence by avoiding local optima, which is a typical difficulty in meta-heuristic optimization. The unpredictability generated by Eqs. (34) and (41) substantially enhances the exploration of the solution space.

5.8.2 Function of pulmonary circulation in avoiding local optima

The most vulnerable people experience significant random disturbances via the pulmonary circulation mechanism. This phase not only diversifies the population but also improves the algorithm's capacity to recover from unfavorable conditions. This method elucidates why BCSBO surpasses other algorithms in high-dimensional

Table 12 Optimal results for the IEEE 118-bus test system

Method	Min	Mean	Max	Std.	Time (s)
EHO	104718.1283	106539.7905	115992.1074	2969	802
TEO	104823.7500	107126.8526	116137.3396	4718	645
MFO	103475.9051	104084.2190	104659.0642	1093	743
PSO	103412.6234	103640.4237	104217.5584	318.6	485
CSBO	103385.6130	103528.1593	103605.8941	75.25	531
BCSBO	103381.0729	103415.9315	103479.6277	45.36	518

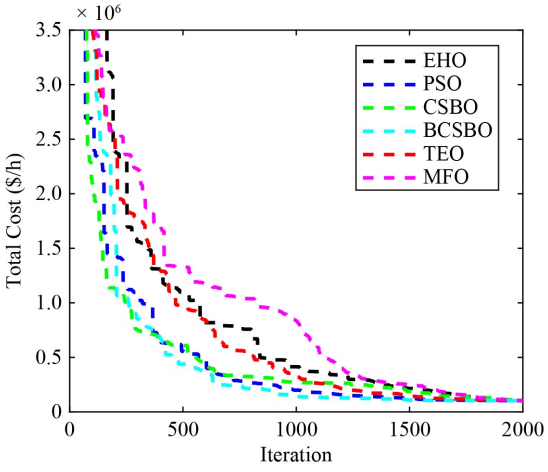

Fig. 12 Convergence trajectories of different methods for the IEEE 118-bus test system.

or intricate issues, as seen by test cases like the IEEE 30-bus and IEEE 118-bus systems. The random variation in these phases helps to explore uncharted portions of the solution space and hence increases the resilience of the method.

5.8.3 Function of systemic circulation in exploitation

The methodical circulation guarantees the refinement of the most promising solutions, hence enhancing convergence speed and accuracy. By establishing a balance between exploration and exploitation, the algorithm efficiently constricts the search area during the latter phases of optimization. This characteristic is apparent in the accelerated convergence patterns of BCSBO relative to other algorithms, as seen in Figs. 7 and 12. The optimization framework's capacity to refine solutions throughout the systemic circulation phase facilitates superior outcomes with less computing expenditure.

5.8.4 Tackling the OPF challenge with renewable energy sources

The integration of RESs into OPF optimization presents considerable challenges owing to the intrinsic fluctuation and uncertainty associated with renewable power supply. BCSBO solves this difficulty by constantly modifying its search method using the circulatory system-inspired model, guaranteeing that optimum solutions may be identified even in complicated systems. The algorithm's adaptability and efficacy are essential for addressing OPF issues related to RESs, where optimization must reconcile renewable energy with grid stability.

5.8.5 Scalability trade-offs

The BCSBO method demonstrates superior performance in smaller-scale systems; nevertheless, its computational expense somewhat escalates in bigger systems owing to the intricacies involved in simulating several circulatory phases. This phenomenon is seen in the IEEE 118-bus system, where the temporal complexity surpasses that of more straightforward algorithms like as PSO and MFO. The enhanced accuracy and better convergence properties in addressing OPF issues with RESs validate this trade-off in situations when solution quality is paramount. The BCSBO's capacity to cope with large-scale difficulties while retaining high performance underscores its promise for real-world applications, notably in integrating RESs into power grids.

5.8.6 Comparison with alternative optimization methods

The findings from the IEEE 30-bus and IEEE 118-bus systems indicate that BCSBO surpasses conventional algorithms, including EHO, TEO, MFO, PSO, and its precursor, CSBO. The comparisons were conducted using five distinct objective functions, and BCSBO shown better performance regarding solution quality and computing efficiency. The efficacy of BCSBO is especially remarkable in addressing the complexity posed by RESs, underscoring its promise as a viable solution for contemporary OPF challenges.

BCSBO offers a unique ability to balance exploration and exploitation by integrating biological factors like pulmonary and systemic circulation into the optimization process. This dual approach explains why it outperforms traditional algorithms in tackling a range of optimization problems, particularly those involving the integration of

renewable energy sources into power networks.

The BCSBO method, although exhibiting robust performance in several optimization situations, has drawbacks characteristic of meta-heuristic algorithms. These encompass:

• **Selection of control parameters**

BCSBO necessitates the meticulous selection of certain control parameters by the user. The algorithm's effectiveness may be contingent upon the values of these parameters, necessitating experimentation or previous knowledge to identify the ideal parameter configuration for each task.

• **Scalability in high-dimensional situations**

Although BCSBO is proficient for small to medium-sized issues, similar to other meta-heuristic algorithms, it may encounter difficulties when addressing very complicated or high-dimensional situations. The approach may need more improvements, including hybridization with other techniques, to improve its scalability and get superior performance in certain instances.

• **Requirement for additional enhancements in specific situations**

In cases of especially complex optimization problems, such as those with extensive search spaces or highly nonlinear systems, BCSBO may not consistently provide the most optimum solutions. Ongoing study and enhancement are essential to modify the algorithm for these more complex conditions.

These limits show that although BCSBO is a viable strategy for many issues, there may be cases where more study or hybridization with other approaches would be useful to maximize performance.

6 Conclusions

Addressing the OPF problem with RESs poses a significant challenge for various algorithms, particularly in complex systems. This paper introduces the BCSBO algorithm as a solution for OPF with RESs, considering five different objective functions. The effectiveness of the suggested BCSBO technique is evaluated using the IEEE 30 test and the IEEE 118-bus test systems and compared against EHO, TEO, MFO, PSO, and CSBO algorithms. The simulation results demonstrate that suggested CSBO is an effective and powerful method for addressing the OPF problem with RESs in power systems. In future research, the BCSBO algorithm will be further utilized to solve the OPF, incorporating FACTs devices. The suggested BCSBO algorithm has considerable promise for future study and applications in many scientific and technical domains. It is adaptable for many optimization problems, including function optimization, mechanical engineering issues, and medicinal applications like for learning machine (Jin et al., 2019), for diagnosis of brain disease (Fei et al., 2020), and prediction of recurrent spontaneous abortion (Shi et al., 2022). Furthermore, expansions of the technique may be investigated, including the creation of fuzzy, binary, and multi-objective variations. Furthermore, the BCSBO algorithm may be integrated with other sophisticated optimization methods to augment its performance and efficiency, hence expanding the horizons of optimization study. These instructions underscore the flexibility and adaptability of the BCSBO algorithm, enabling new applications and progress across several fields.

Competing Interests The authors declare that they have no competing interests.

References

Abdo M, Kamel S, Ebeed M, Yu J, Jurado F (2018). Solving non-smooth optimal power flow problems using a developed grey wolf optimizer. Energies, 11(7): 1692

Abid M, Belazzoug M, Mouassa S, Chanane A, Jurado F (2024a). Optimal power flow of thermal-wind-solar power system using enhanced Kepler optimization algorithm: Case study of a large-scale practical power system. Wind Engineering, 48(5): 708–739

Abid M, Belazzoug M, Mouassa S, Chanane A, Jurado F (2024b). Multi-objective optimal power flow analysis incorporating renewable energy sources and FACTS devices using non-dominated sorting kepler optimization algorithm. Sustainability, 16(21): 9599

Ahmad M, Javaid N, Niaz I A, Almogren A, Radwan A (2021). A bio-inspired heuristic algorithm for solving optimal power flow problem in hybrid power system. IEEE Access: Practical Innovations, Open Solutions, 9: 159809–159826

Ahmadi A, Ahmadi M R, Nezhad A E (2014). A lexicographic optimization and augmented ϵ-constraint technique for short-term environmental/economic combined heat and power scheduling. Electric Power Components and Systems, 42(9): 945–958

Alanazi A, Alanazi M, Memon Z A, Mosavi A (2022). Determining optimal power flow solutions using new adaptive Gaussian TLBO method. Applied Sciences, 12(16): 7959

Alghamdi A S (2023). Optimal power flow of hybrid wind/solar/thermal energy integrated power systems considering costs and emissions via a novel and efficient search optimization algorithm. Applied Sciences, 13(8): 4760

Alghamdi A S, Zohdy M A (2024). Boosting cuckoo optimization algorithm via Gaussian mixture model for optimal power flow

problem in a hybrid power system with solar and wind renewable energies. Heliyon, 10(11): e31755

Belagra E A, Mouassa S, Chettih S, Jurado F (2024). Optimal power flow calculation in hybrid power system involving solar, wind, and hydropower plant using weighted mean of vectors algorithm. Wind Engineering, 48(3): 468–493

Biswas P P, Suganthan P N, Amaratunga G A J (2017). Optimal power flow solutions incorporating stochastic wind and solar power. Energy Conversion and Management, 148: 1194–1207

Biswas P P, Suganthan P N, Mallipeddi R, Amaratunga G A J (2018). Optimal power flow solutions using differential evolution algorithm integrated with effective constraint handling techniques. Engineering Applications of Artificial Intelligence, 68: 81–100

Charwand M, Ahmadi A, Sharaf A M, Gitizadeh M, Esmaeel Nezhad A (2016). Robust hydrothermal scheduling under load uncertainty using information gap decision theory. International Transactions on Electrical Energy Systems, 26(3): 464–485

Chen G, Qian J, Zhang Z, Sun Z (2019a). Multi-objective optimal power flow based on hybrid firefly-bat algorithm and constraints-prior object-fuzzy sorting strategy. IEEE Access: Practical Innovations, Open Solutions, 7: 139726–139745

Chen M R, Zeng G Q, Lu K D (2019b). Constrained multi-objective population extremal optimization based economic-emission dispatch incorporating renewable energy resources. Renewable Energy, 143: 277–294

Duman S, Rivera S, Li J, Wu L (2020). Optimal power flow of power systems with controllable wind-photovoltaic energy systems via differential evolutionary particle swarm optimization. International Transactions on Electrical Energy Systems, 30(4): e12270

Esmaeel Nezhad A, Jowkar S, Tavakkoli Sabour T, Rahimi E, Ghanavati F, Esmaeilnezhad F (2024a). A short-term wind-hydrothermal operational framework in the presence of pumped-hydro storage. e-Prime — Advances in Electrical Engineering, Electronics and Energy, 8: 100577

Esmaeel Nezhad A, Mobtahej M, Javadi M S, Nardelli P H J, Sahoo S (2024b). Optimal operation of lithium-ion batteries in microgrids using a semidefinite thermal model. International Journal of Electrical Power & Energy Systems, 155: 109630

Esmaeel Nezhad A, Rahimnejad A, Nardelli P H J, Gadsden S A, Sahoo S, Ghanavati F (2022). A shrinking horizon model predictive controller for daily scheduling of home energy management systems. IEEE Access: Practical Innovations, Open Solutions, 10: 29716–29730

Esmaeel Nezhad A, Tavakkoli Sabour T, Javadi M S H.J, Nardelli P, Jowkar S, Ghanavati F (2025). Water–energy nexus. In: Tostado-Véliz M, Rezaee Jordehi A, Mansouri S A, Ramos A, Jurado F, eds. Towards Future Smart Power Systems with High Penetration of Renewables. Academic Press, 75–102

Fei X, Wang J, Ying S, Hu Z, Shi J (2020). Projective parameter transfer based sparse multiple empirical kernel learning machine for diagnosis of brain disease. Neurocomputing, 413: 271–283

Ghasemi M, Akbari E, Faraji Davoudkhani I, Rahimnejad A, Asadpoor M B, Gadsden S A (2022a). Application of Coulomb's and Franklin's laws algorithm to solve large-scale optimal reactive power dispatch problems. Soft Computing, 26(24): 13899–13923

Ghasemi M, Akbari M A, Jun C, Bateni S M, Zare M, Zahedi A, Pai H, Band S S, Moslehpour M, Chau K (2022b). Circulatory system based optimization (CSBO): An expert multilevel biologically inspired meta-heuristic algorithm. Engineering Applications of Computational Fluid Mechanics, 16(1): 1483–1525

Ghasemi M, Davoudkhani I F, Akbari E, Rahimnejad A, Ghavidel S, Li L (2020). A novel and effective optimization algorithm for global optimization and its engineering applications: Turbulent flow of water-based optimization (TFWO). Engineering Applications of Artificial Intelligence, 92: 103666

Ghasemi M, Ghavidel S, Gitizadeh M, Akbari E (2015). An improved teaching–learning-based optimization algorithm using Lévy mutation strategy for non-smooth optimal power flow. International Journal of Electrical Power & Energy Systems, 65: 375–384

Ghasemi M, Trojovský P, Trojovská E, Zare M (2023a). Gaussian bare-bones Levy circulatory system-based optimization for power flow in the presence of renewable units. Engineering Science and Technology, An International Journal, 47: 101551

Ghasemi M, Zare M, Kadkhoda Mohammadi S, Mirjalili S (2024a). Applications of whale migration algorithm in optimal power flow problems of power systems (2024a). In: Mirjalili S, ed. Handbook of Whale Optimization Algorithm: Variants, Hybrids, Improvements, and Applications. Academic Press, 347–64

Ghasemi M, Zare M, Zahedi A, Akbari M, Mirjalili S, Abualigah L (2023b). Geyser inspired algorithm: A new geological-inspired meta-heuristic for real-parameter and constrained engineering optimization. Journal of Bionic Engineering, 1–35

Ghasemi M, Zare M, Zahedi A, Trojovský P, Abualigah L, Trojovská E (2024b). Optimization based on performance of lungs in body: Lungs performance-based optimization (LPO). Computer Methods in Applied Mechanics and Engineering, 419: 116582

Guvenc U, Duman S, Kahraman H T, Aras S, Katı M (2021). Fitness–Distance Balance based adaptive guided differential evolution algorithm for security-constrained optimal power flow problem incorporating renewable energy sources. Applied Soft Computing, 108: 107421

Hassan M H, Elsayed S K, Kamel S, Rahmann C, Taha I B M (2022). Developing chaotic Bonobo optimizer for optimal power flow analysis considering stochastic renewable energy resources. International Journal of Energy Research, 46(8): 11291–11325

Hassan M H, Kamel S, Selim A, Khurshaid T, Domínguez-garcía J L (2021). A modified rao-2 algorithm for optimal power flow incorporating renewable energy sources. Mathematics, 9(13): 1532

Houssein E H, Oliva D, Samee N A, Mahmoud N F, Emam M M (2023). Liver cancer algorithm: A novel bio-inspired optimizer. Computers in Biology and Medicine, 165: 107389

Javadi M S, Nezhad A E, Gough M, Lotfi M, Anvari-Moghaddam A, Nardelli P H J, Sahoo S, Catalão J P S (2021). Conditional value-at-risk model for smart home energy management systems. e-Prime-Advances in Electrical Engineering, Electronics and Energy, 1: 100006

Jin X, He T, Lin Y (2019). Multi-objective model selection algorithm for online sequential ultimate learning machine. EURASIP Journal on Wireless Communications and Networking, 2019(1): 1–7

Kathiravan R, Kumudini Devi R P (2017). Optimal power flow model incorporating wind, solar, and bundled solar-thermal power in the restructured Indian power system. International Journal of Green

Energy, 14(11): 934–950

Kaveh A, Dadras A (2017). A novel meta-heuristic optimization algorithm: Thermal exchange optimization. Advances in Engineering Software, 110: 69–84

Kouadri R, Mouassa S, Jurado F (2024). Optimal power dispatch in hybrid power system for medium-and large-scale practical power systems using self-adaptive bonobo optimizer algorithm. Wind Engineering, 48(6): 1118–1140

Li S, Chen H, Wang M, Heidari A A, Mirjalili S (2020). Slime mould algorithm: A new method for stochastic optimization. Future Generation Computer Systems, 111: 300–323

Lian J, Hui G, Ma L, Zhu T, Wu X, Heidari A A, Chen Y, Chen H (2024). Parrot optimizer: Algorithm and applications to medical problems. Computers in Biology and Medicine, 172: 108064

Mirjalili S (2015). Moth-flame optimization algorithm: A novel nature-inspired heuristic paradigm. Knowledge-Based Systems, 89: 228–249

Mohamed A A A, Mohamed Y S, El-Gaafary A A M, Hemeida A M (2017). Optimal power flow using moth swarm algorithm. Electric Power Systems Research, 142: 190–206

Mouassa S, Alateeq A, Alassaf A, Bayindir R, Alsaleh I, Jurado F (2024). Optimal power flow analysis with renewable energy resource uncertainty using dwarf mongoose optimizer: Case of Adrar isolated electrical network. IEEE Access: Practical Innovations, Open Solutions, 12: 10202–10218

Mouassa S, Althobaiti A, Jurado F, Ghoneim S S M (2022). Novel design of slim mould optimizer for the solution of optimal power flow problems incorporating intermittent sources: A case study of Algerian electricity grid. IEEE Access: Practical Innovations, Open Solutions, 10: 22646–22661

Mouassa S, Bouktir T (2015). Artificial bee colony algorithm for solving OPF problem considering the valve point effect. International Journal of Computer Applications, 112(1)

Mouassa S, Makhloufi S, Djabali C, Jurado F (2023). Optimal power flow solution based on gorilla troops optimization technique considering uncertainty of renewable energy sources: A case study of Adrar's isolated power network. Wind Engineering, 47(5): 913–934

Muttaqi K M, Esmaeel Nezhad A, Aghaei J, Ganapathy V (2014). Control issues of distribution system automation in smart grids. Renewable & Sustainable Energy Reviews, 37: 386–396

Naderi E, Narimani H, Pourakbari-Kasmaei M, Cerna F V, Marzband M, Lehtonen M (2021). State-of-the-art of optimal active and reactive power flow: A comprehensive review from various standpoints. Processes, 9(8): 1319

Nezhad A E, Nardelli P H J, Sahoo S, Ghanavati F (2022). Scheduling of energy hub resources using robust chance-constrained optimization. IEEE Access: Practical Innovations, Open Solutions, 10: 129738–129753

Nguyen T T (2019). A high performance social spider optimization algorithm for optimal power flow solution with single objective optimization. Energy, 171: 218–240

Niknam T, Narimani M R, Aghaei J, Tabatabaei S, Nayeripour M (2011). Modified honey bee mating optimisation to solve dynamic optimal power flow considering generator constraints. IET Generation, Transmission & Distribution, 5(10): 989–1002

Razavi S E, Esmaeel Nezhad A, Mavalizadeh H, Raeisi F, Ahmadi A (2018). Robust hydrothermal unit commitment: A mixed-integer linear framework. Energy, 165: 593–602

Saddique M S, Bhatti A R, Haroon S S, Sattar M K, Amin S, Sajjad I A, Ul Haq S S, Awan A B, Rasheed N (2020). Solution to optimal reactive power dispatch in transmission system using meta-heuristic techniques—Status and technological review. Electric Power Systems Research, 178: 106031

Salkuti S R (2019). Optimal power flow using multi-objective glowworm swarm optimization algorithm in a wind energy integrated power system. International Journal of Green Energy, 16(15): 1547–1561

Sarda J, Pandya K, Lee K Y (2023). Hybrid cross entropy—Cuckoo search algorithm for solving optimal power flow with renewable generators and controllable loads. Optimal Control Applications & Methods, 44(2): 508–532

Sarhan S, El-Sehiemy R, Abaza A, Gafar M (2022). Turbulent flow of water-based optimization for solving multi-objective technical and economic aspects of optimal power flow problems. Mathematics, 10(12): 2106

Shi B, Chen J, Chen H, Lin W, Yang J, Chen Y, Wu C, Huang Z (2022). Prediction of recurrent spontaneous abortion using evolutionary machine learning with joint self-adaptive sime mould algorithm. Computers in Biology and Medicine, 148: 105885

Su H, Zhao D, Heidari A A, Liu L, Zhang X, Mafarja M, Chen H (2023). RIME: A physics-based optimization. Neurocomputing, 532: 183–214

Ullah Z, Wang S, Radosavljevic J, Lai J (2019). A solution to the optimal power flow problem considering WT and PV generation. IEEE Access: Practical Innovations, Open Solutions, 7: 46763–46772

Wang G G, Deb S, Coelho L D S (2016). Elephant herding optimization. In: Proceedings 2015 3rd International Symposium on Computational and Business Intelligence, ISCBI 2015. Indonesia, 1–5

Yang Y, Chen H, Heidari A A, Gandomi A H (2021). Hunger games search: Visions, conception, implementation, deep analysis, perspectives, and towards performance shifts. Expert Systems with Applications, 177: 114864

Zahedibialvaei A, Trojovský P, Hesari-Shermeh M, Matoušová I, Trojovská E, Hubálovský Š (2023). An enhanced turbulent flow of water-based optimization for optimal power flow of power system integrated wind turbine and solar photovoltaic generators. Scientific Reports, 13(1): 14635

Zimmerman R D, Murillo-Sánchez C E, Thomas R J (2011). MATPOWER: Steady-state operations, planning, and analysis tools for power systems research and education. IEEE Transactions on Power Systems, 26(1): 12–19